

Multi-annual Study of Chlorine Species in the Stratosphere using Airborne Microwave Measurements

A Thesis Submitted by

Yakub Adesoga Tijani

to

The Graduate School for the Degree of Master of Science in Environmental
Physics

**Institute of Environmental Physics
University of Bremen, Germany**

December 2004

Declaration

I hereby declare that I did the written work on my own and only with the means as indicated.

.....

Date and Signature

CONTENTS

Introduction	4
1. CHEMISTRY AND DYNAMICS OF THE STRATOSPHERE	9
1.1 Vertical Structure of the Earth's Atmosphere	9
1.2 Composition of the Earth's atmosphere	12
1.3 Dynamic and transport processes	14
1.3.1 Brewer-Dobson Circulation	14
1.3.2 The Polar Vortex	16
1.3.3 Potential Vorticity	17
1.4 Chemistry of the Stratosphere	19
1.4.1 The Chapman Cycle	19
1.4.2 Catalytic Reactions	21
1.4.3 Polar Stratospheric Clouds	23
1.4.4 Chlorine Chemistry and Heterogenous Reactions in the Polar Stratosphere	25
1.4.5 Denitrification	30
2. MICROWAVE MEASUREMENT TECHNIQUES	31
2.1 Radiative Transfer	31
2.1.1 Radiative Transfer Equation	32
2.1.2 Brightness Temperature	35
2.2 Line Broadening and Intensity	36
2.2.1 Line Shape	36
2.2.2 Line Strength	41
2.2.3 Absorption Coefficient	42
2.2.4 Continuum Absorption	42
2.3 The Airborne Submillimeter Radiometer	43

2.3.1	Heterodyne Principle	44
2.3.2	Calibration	46
2.3.3	Instrumental Assembly	48
2.3.4	Spectrometers	52
3	RETRIEVAL AND ANALYSIS OF DATA	54
3.1	Optimal Estimation Method	54
3.1	Analyses of retrieval errors and altitude resolution	58
3.2	Retrieval and analyses of ASUR's ClO, HCl and Ozone	63
4	RESULTS	
4.1	Meteorological Conditions	72
4.2	General Overview of ASUR's ClO and HCl measurements between 1995 and 2003	74
4.3	Seasonal variation of ASUR's ClO and HCl measurements	80
4.4	Latitudinal variation of ASUR's ClO and HCl measurements	82
4.5	Comparisons of ASUR's ClO with other instruments and model results	85
4.6	Discussion and Conclusions	88
	SUMMARY	90
	ACKNOWLEDGEMENT	91
	REFERENCES	92

INTRODUCTION

The seasonal phenomenon of the Antarctic ozone hole (Farman et al,1985) immediately raises the question of whether similar losses can take place in the Arctic during late winter and spring period, despite the remarkable differences in meteorological conditions in the two hemispheres. The scientific evidence, accumulated over more than two decades of study by the international research community, has shown that anthropogenic emissions are responsible for the observed depletions of the ozone layer over Antarctica and likely play a major role in global ozone losses (WMO,1994). These emissions are traced to Chlorofluorocarbons (CFCs). They are nontoxic, nonflammable compounds containing atoms of carbon, chlorine, and fluorine. CFCs were first synthesized in the 19th century and achieved a widespread industrial use as refrigerants, propellants and solvents among other applications. However, the lack of chemical reactivity that makes CFC molecules intrinsically useful also provide for them a high degree of immunity against tropospheric removal by oxidation, photodissociation or wet and dry deposition. The major sink for most of them is by photolysis in the stratosphere (Molina and Rowland,1974) by solar ultraviolet radiation. This creates a reservoir of chlorine compounds in the stratosphere. Furthermore, the absence of sunlight in polar winter produces a low pressure system, the so called polar vortex, with very low temperatures. The low temperatures lead to the formation of polar stratospheric clouds (PSCs).

Reactive chlorine can be formed from the chlorine reservoir species by heterogeneous reactions in the solid or liquid phase of particles of polar stratospheric clouds . The reactive chlorine then causes rapid ozone loss by a catalytic cycle when sunlight reaches the polar stratosphere. In view of the above and as shown in Fig. A, production of CFCs has to be regulated, otherwise the impact will be catastrophic for many generations to come. Results have been achieved by the Montreal Protocol in 1987 and its subsequent amendments.

Although some chemical transport models (CTMs), forced by meteorological analyses, can successfully reproduce the general features of the seasonal evolution of total column ozone and show good agreement between model and observed ozone depletion (e.g Sinnhuber et al., 2000), models still fail to reproduce many aspects of polar chemistry and transport, especially in the Arctic. This is partly due to significant year-to-year variability in Arctic meteorology with subsequent interannual variability in the polar ozone loss (Chipperfield and Jones,1999). Other causes are uncertainties in the chemical reaction rates and the process of denitrification which removes HNO_3 from the polar stratosphere by sedimentation of PSC particles (Kleinböhl et al., 2002), leading to prolonged ozone destruction.

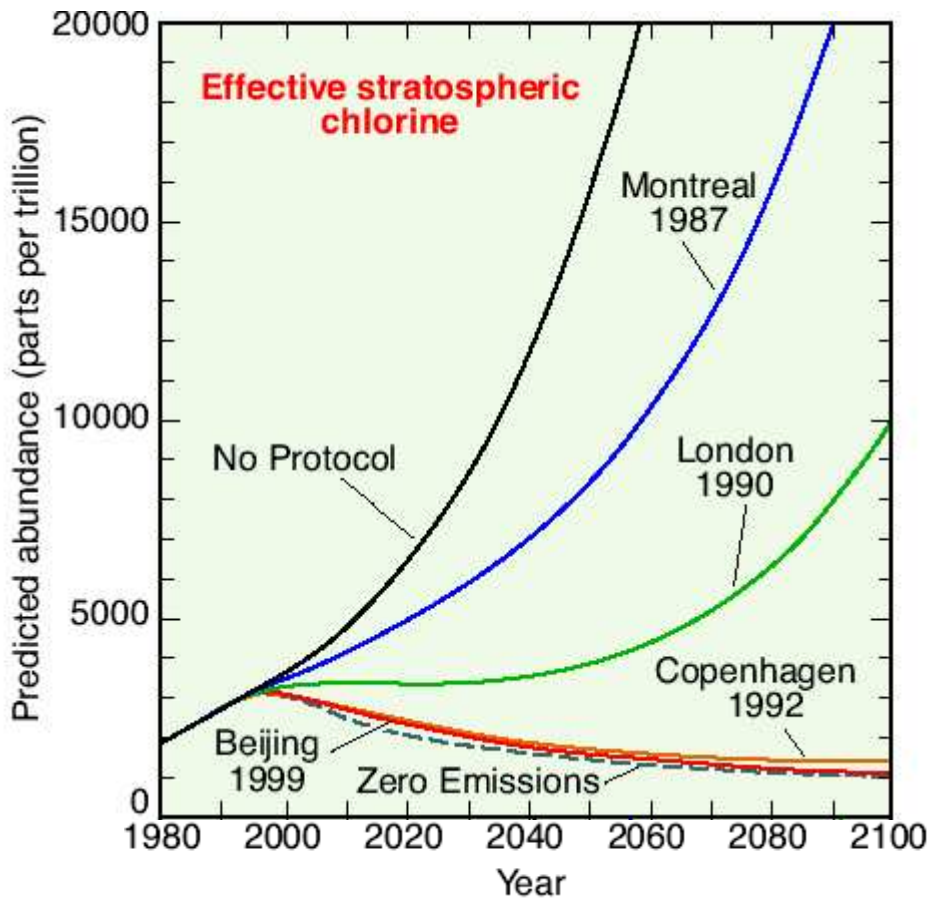


Fig. A. The projected decadal distribution of chlorine in the stratosphere with and without regulations. (WMO,1994)

Thus, model calculations of constituents in polar region is masked by dynamic variability caused by vertical and horizontal advection and by mixing of air masses (Grooß and Müller, 2003). Furthermore, the understanding of how changes in halogen and aerosol loading affect ozone suggests some of the reasons for the unsuitability of using a linear extrapolation of the pre-1991 ozone trend to the present, thereby giving rise to the relevance of a multi-annual investigation of chlorine species and ozone.

This study is aimed at investigating some of these chlorine species by analyzing a time series of ClO and HCl between 1995 and 2003 from microwave measurements. The data used for this investigation is from measurements carried out by the Airborne Submillimeter Radiometer, ASUR. It is a heterodyne receiver developed in the early 1990s by the Institute of Environmental Physics, University of Bremen, Germany, and upgraded in 1994 with a superconducting mixer developed by the Space Research Organisation of the Netherlands (SRON, Groningen, The Netherlands). It is capable of measuring vertical profiles of several stratospheric trace gases relevant to polar stratospheric ozone chemistry by detecting thermal emission lines of the molecules in the 604.3 - 662.3 GHz spectral range. The main target species of the instrument are ozone, the reactive chlorine species ClO - which is very efficient for catalytic ozone destruction in the lower stratosphere, the chlorine reservoir gas HCl, the important constituent of polar stratospheric clouds - HNO₃, and the chemically inert tracer N₂O - suitable to differentiate between chemical and dynamical processes. ASUR also detects spectral features of several other minor trace gases.

The instrument was used during several campaigns in almost yearly intervals between 1991 and 2003 to investigate the chemical composition of the arctic and mid-latitude winter stratosphere. ASUR successfully participated, on board the German research aircraft Falcon in the European Arctic field campaigns (EASOE 1991/1992), MLS / UARS validation (1993), SESAME (1994/1995), GOME / ERS-2 validation (1996), ILAS / ADEOS validation (1997), THESEO / HIMSPEC (1999), European Polar

Stratospheric Cloud and Lee wave Experiment (EUPLEX 2003) and Sciamachy Validation and Utilisation Experiment (SCIA-VALUE 2002/2003). Also on board the NASA research aircraft DC-8, the instrument took part in the SAGE III Ozone loss and validation experiment (SOLVE 1999/2000) and the pacific LEONID Multi-instrument Aircraft Campaign (2002).

All the winters showed differences in their development in terms of dynamics and temperatures. In chapter 1, an overview of the atmospheric vertical profile and composition is given, followed by the dynamical processes and chemistry in the polar stratosphere. Chapter 2 discusses the measurement techniques used in microwave remote sensing vis-à-vis the radiative transfer of the electromagnetic radiation. Last section of chapter 2 focuses on the ASUR instrument as a typical example of a microwave instrument. In chapter 3, a description of the retrieval method is given, while the data and error analyses are presented. Chapter 4 explains and discusses the results of this research work after briefly describing the meteorological conditions that existed in all the considered winters.

1. CHEMISTRY AND DYNAMICS OF THE STRATOSPHERE

1.1 VERTICAL STRUCTURE OF THE EARTH'S ATMOSPHERE

The Earth's atmosphere can be divided into a number of atmospheric layers according to its thermal structure. This structure is not uniform, but instead behaves in different ways in different layers of the atmosphere. These differences are associated with the chemistry, composition, and density of the atmosphere at different levels. The atmosphere is characterized by an exponentially decreasing pressure and density, with increasing altitude. As shown in Figure 1.1, the vertical profile can be divided into four distinct layers: troposphere, stratosphere, mesosphere and thermosphere. These are separated by transition regions: tropopause, stratopause and mesopause, respectively.

The troposphere is the lowest layer of the earth's atmosphere. It is characterized by strong vertical mixing but a negative temperature gradient, decreasing temperature with increasing altitude, thereby becoming inherently vertically unstable. The troposphere contains about 80% of the mass of Earth atmosphere, and almost all the water vapor, clouds and precipitation. The negative temperature gradient holds until the tropopause

where a minimum temperature is reached. The altitude and temperature of the tropopause varies with latitude and season. It is located at around 8 km and 10 km in polar regions and at mid latitudes respectively, while in the tropics, it is usually located at altitudes between 14 and 16 km. Also, tropopause height is proportional to mean tropospheric temperature: higher in summer, lower in winter.

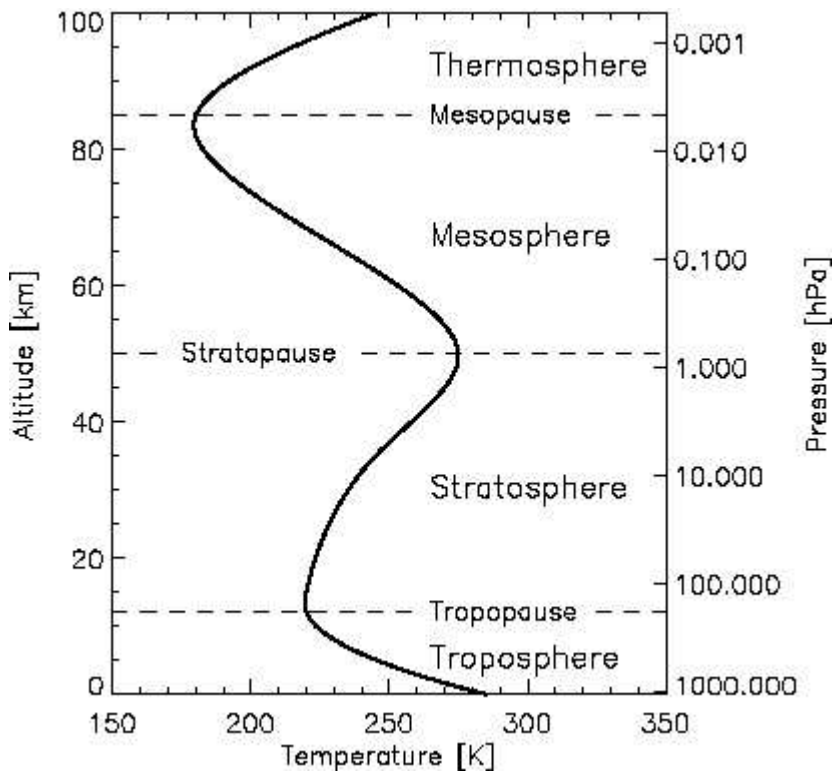


Figure 1.1: Vertical temperature profile of the atmosphere, adapted from Kleinböhl, 2003

The stratosphere extends from the tropopause to an altitude of about 50 km. It is an inversion layer showing an increase of temperature with altitude. Because temperature rises with height in the stratosphere, the condition of warmer air above colder air exists.

This makes the stratosphere convectively stable with respect to vertical motion, resulting in little vertical mixing, and long residence times of constituents. Inversion of temperature between stratosphere and troposphere is also preventing mixing between the two layers. The positive temperature gradient in the stratosphere is a consequence of heating due to the absorption of solar ultra-violet radiation by stratospheric ozone. The increase in temperature with altitude changes at the stratopause and the mesosphere begins above. Although, vertical motions are often small in the stratosphere, horizontal motions can be very rapid.

The mesosphere contains about 0.099% of the atmospheric mass. Bounded by the stratopause from below and the mesopause from above, it exhibits a negative temperature gradient. The decrease of mesospheric temperature with altitude reaches up to the mesopause at around 90 km altitude, where in the polar summer the lowest temperatures of the Earth's atmosphere can be found. The temperature can become so low that clouds – Noctilucent Clouds, will form at these altitudes despite the very low water vapour content.

The thermosphere or ionosphere contains 0.001% of the atmospheric mass. Here, the temperature shows a strong increase again. It is caused by absorption of solar ultra-violet radiation by molecular oxygen, which strongly depends on solar activity. The strong temperature increase in the thermosphere is also due to little radiative cooling and small amount of energy exchange between molecules because of the low air density.

1.2 COMPOSITION OF THE EARTH'S ATMOSPHERE

The major constituents of the atmosphere are molecular nitrogen N_2 , molecular oxygen O_2 and a small contribution of noble gases. Shown in Table 1.1 is an inexhaustive distribution of gases in the atmosphere. About 99% of the air is composed of nitrogen and oxygen. The remaining 1% of the atmosphere consists of argon Ar and trace constituents among which are water vapor, carbon dioxide, ozone, methane and noble gases. They are called trace gases because they exist in small amounts. The most frequently used units for giving the VMR of these minor atmospheric species are:

$$1 \cdot 10^{-6} = 1 \text{ ppm (part per million)}$$

$$1 \cdot 10^{-9} = 1 \text{ ppb (part per billion)}$$

$$1 \cdot 10^{-12} = 1 \text{ ppt (part per trillion)}$$

Based on chemical composition, the atmosphere can be divided into two broad regions: homosphere and heterosphere. In the homosphere, nitrogen and oxygen are uniformly mixed because of winds, convection and circulation patterns. Thus, stratification by weight does not occur and there is thermodynamical equilibrium. This region extends from the surface to approximately 100 km. Above 100 km, oxygen and nitrogen are not uniformly mixed. This is because the different gases that make up the air begin to separate (stratify) according to their molecular weight. Lighter gases accelerate with altitude. The heterosphere is the outer region where nitrogen and

Atmospheric constituents	Volume mixing ratio in air
Nitrogen	0.7808
Oxygen	0.2095
Argon	0.0093
Water vapor	0-0.04
Carbon dioxide	325×10^{-6}
Ozone	$0 - 12 \times 10^{-6}$
Chlorine monoxide	$0 - 1.8 \times 10^{-9}$
Methane	1.7×10^{-6}
Hydrogen	500×10^{-9}
Noble gases	2.4×10^{-6}

Table 1.1: Distribution of gases in the atmosphere (courtesy of different literature values)

more than heavier gases, and at around 100km, the air is so thin that individual molecules are able to accelerate to very high speeds before bumping into another molecule. Thus, there is no thermodynamical equilibrium in the heterosphere.

1.3 DYNAMIC AND TRANSPORT PROCESSES

Dynamic and transport processes refer to winds and broad circulation patterns that move parcels of air mass. These processes play an indirect role in the upper stratosphere because of the impact they have on the temperature structure which in turn affects the amount of constituents. However in the lower stratosphere, knowledge of transport is fundamental to determine the basic distribution of stratospheric constituents.

1.3.1 Brewer-Dobson circulation

The central concept in stratospheric transport is the Brewer-Dobson circulation which governs the vertical and meridional motion in the lower stratosphere. It is a slow circulation that moves atmospheric constituents from the tropics into the middle and polar latitudes. As shown in fig. 1.2, it involves the rising of air mass in the tropics, drifting of the air mass towards the pole and a descent at polar latitudes in the stratosphere. This explains, for example, why tropical air is lower in ozone than polar air, even though the source region of

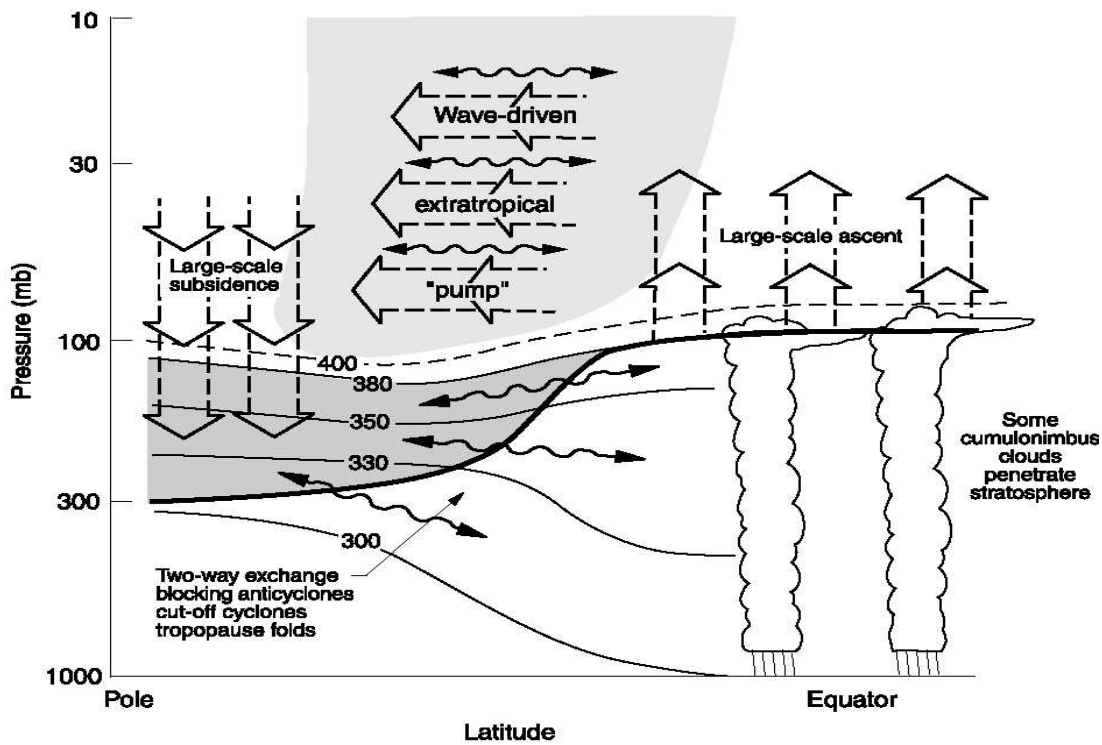


Figure 1.2: Dynamic aspect of stratosphere-troposphere exchange (Holton et al., 1995). The broad arrows show Brewer-Dobson circulation. Thin lines indicate surfaces of constant potential temperatures. The thick line shows the tropopause while tropopause folding occurs in the shaded part of the stratosphere.

ozone is in the tropics. The driving force for Brewer-Dobson circulation is the breaking of planetary waves in the winter hemisphere. The planetary waves are caused by combination of large-scale topographical features, meridional temperature gradients and rotation of the Earth that produces Coriolis deflection. Furthermore, the breaking of these planetary waves causes a drag force that drives the meridional transport circulation in the stratosphere. However, some of the stratospheric air may get into the troposphere through a process called tropopause folding. It involves an intrusion of a thin band of

stratospheric air into the troposphere along strongly tilted surfaces of constant potential temperature.

1.3.2 The Polar Vortex

The Polar vortex is a large-scale cyclonic circulation in the stratosphere centred generally in the polar regions. It is a low-pressure system formed as a result of low temperatures due to radiative cooling and absence of heating by solar radiation in the polar stratosphere during winter. This is a consequence of high temperature difference between mid latitude and polar regions, leading to the development of polar night jet – a meridional motion which is changed to a zonal wind by the coriolis force. The polar vortex isolates polar airmasses from mid-latitude air because of its high wind velocities that prevent horizontal exchange of air masses inside and outside the vortex. The degree of isolation generally varies between the Arctic and Antarctic due to the difference in their topographies. Because the Antarctic is surrounded by oceans, this allows a better circulation of zonal winds and results in a stable and persistent vortex with very low temperatures. In contrast, zonal circulation is disturbed by land masses and orographic features in the northern hemisphere. These induced planetary scale wave activities leading to higher temperatures, less persistence and reduced stability in the Arctic vortex compared to the Antarctic vortex.

1.3.3 Potential Vorticity

Potential vorticity provides a very powerful dynamic tool. It is used to distinguish stratospheric air that is inside or outside of the polar vortex. Under an adiabatic and frictionless movement of airmass, potential vorticity (PV) is defined as the product of absolute vorticity (a measure of rotation of horizontally moving air about a point) and static stability on a constant potential temperature surface. This is expressed as:

$$PV = (\zeta_{\theta} + f) \left(-g \frac{\partial \theta}{\partial p} \right) \quad 1.1$$

where θ is the potential temperature, ζ_{θ} the vertical component of relative vorticity evaluated on an isentropic surface (where $\theta = \text{constant}$), f the Coriolis parameter, p the pressure of the airmass and g the gravitational acceleration.

The potential temperature θ is defined as the temperature an air parcel would have if expanded or compressed adiabatically (i.e., without any heat being added or taken away) from its existing pressure p to a reference pressure p_0 , usually taken to be 1000hPa. It is mathematically represented as:

$$\theta = T \left(\frac{p_0}{p} \right)^\kappa \quad 1.2$$

with T the temperature of the air parcel and

$$\kappa = \left(\frac{R}{c_p} \right) \approx \frac{2}{7}$$

R is the gas constant for air, and c_p is the specific heat capacity at constant pressure for air.

The relative vorticity ζ_θ is given as:

$$\zeta_\theta = \vec{k} \cdot \left(\vec{\nabla}_\theta \times \vec{v} \right) \quad 1.3$$

\vec{v} is the windspeed, and the Coriolis parameter f (often called planetary vorticity) is expressed as:

$$f = 2\Omega \sin \phi \quad 1.4$$

Ω is Earth's angular speed of rotation, 7.292×10^{-5} rad/s, and ϕ is the latitude (in radian).

Although the temperature and wind speed of a particular air parcel might vary in time, the potential vorticity remains conserved. Hence it is used to follow the motion of air in the stratosphere, as shown in fig 1.3. Surfaces of constant potential vorticity are called isentropic surfaces.

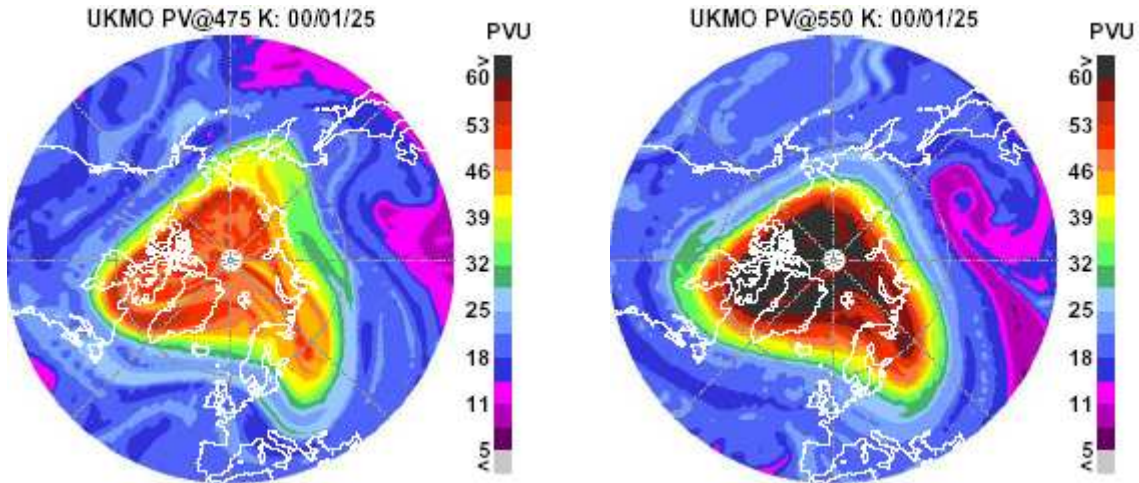


Figure 1.3: Potential Vorticity maps at two different potential temperature levels (450K and 550K) during one of the ASUR campaigns on 25th January 2000 (Courtesy Kai-Uwe Eichmann)

1.4 Chemistry of the Stratosphere

1.4.1 The Chapman cycle

The processes leading to formation and destruction of ozone were first explained in 1930 by Chapman (Chapman, S., 1930). He postulated that ultraviolet radiation was responsible for ozone production and his observations laid the foundation for stratospheric photochemistry known as Chapman reactions. Chapman proposed that

atomic oxygen is formed when O₂ is photodissociated by high energy ultraviolet photons with wavelengths less than or equal to 243nm:



where h is the Planck constant, ν is the frequency of the photon and λ is the wavelength of the photon. Since oxygen atoms are highly reactive, they quickly react with oxygen molecules to form ozone (although they may also recombine to form molecular oxygen again):



M is a reaction partner that remains unchanged in the reaction. It is needed for the energy balance of the reaction. It could be N₂ or O₂. Equation 1.6 proceeds at a very fast rate so that oxygen atoms almost immediately form ozone after they are dissociated in reaction 1.5.

Chapman also hypothesized that ozone can be destroyed by the reaction with atomic oxygen :



The ozone molecule can also be photolyzed into O and O₂ :



However, despite the good concept, Chapman ozone estimates are higher in the tropics and lower in the polar regions than real observations. This is because there are other catalytic reactions with gases containing chlorine, bromine, nitrogen, and hydrogen that contribute to the overall destruction of ozone. Also, as a result of Brewer-Dobson Circulation that transports ozone from the photochemical production region in the tropics to the middle and high latitudes, the Chapman reactions are insufficient to describe photochemistry in the atmosphere.

1.4.2 Catalytic Reactions

A catalyst is a substance that causes chemical reactions without itself being consumed by those reactions. As indicated in previous section, several catalytic cycles that involve other species apart from oxygen can intensify the destruction of ozone. Generally, they have the form:



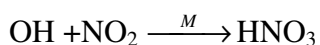
where X is the catalyst and it could be Cl, Br, H, OH or NO. Because X is not consumed, large ozone destruction can occur even if the concentration of X is several orders of magnitude lower than the ozone concentration. However, as this work focuses on chlorine species, subsequent sections will deal with the catalytic reactions involving X as Cl.

The anthropogenic nature of most chlorine in the stratosphere (from chlorofluorocarbons CFCs) cannot be overemphasised (WMO, 1994). Developed in the 1920s as a safe, cheap, nontoxic refrigerant alternative to ammonia, CFC molecules can be transported across the tropopause into the stratosphere because they have very long lifetimes and are not water soluble. Although natural sources of chlorine exist, most of the observed chlorine in the stratosphere at the present time are due to the release of chlorine atoms from the photolysis of CFC molecules. For example, photolysis of CFCl_3 and CF_2Cl_2 will produce the following reactions:



However, several reactions exist that transform these reactive chlorine into reservoir species. Some of these are:





1.20

HCl, HOCl and ClONO₂ are chlorine reservoir species with different lifetimes, determined by their photolysis rates. HCl has the longest lifetime in the order of weeks while HOCl is the shortest, with a lifetime in the order of hours. The reservoir species are mostly unreactive except at certain conditions. These conditions are explained in subsequent sections.

1.4.3 Polar Stratospheric Clouds

Polar stratospheric clouds (PSCs) are formed in the extremely cold and dry conditions that subsist during winter in the polar vortex region of the Antarctic and sometimes in the Arctic stratosphere. They provide the surfaces on which the ozone destroying reactions occur by converting reservoir chlorine species that do not destroy ozone (e.g. HCl and ClONO₂) into reactive forms that can destroy ozone. A considerable presence of PSCs is found every year in the stable vortex of the Antarctic winter, and has also been reported in the Arctic vortex during the last decade. However, the composition of polar stratospheric cloud particles has been investigated using data from several remote sensing instruments including ASUR (von König et al., 2002)

There are two types of PSCs, referred to as Type I and Type II PSCs. Type I is subdivided into Ia and Ib.

Type Ia PSC

Type Ia PSCs are made up of frozen nitric acid trihydrates (NAT- $\text{HNO}_3 \cdot 3\text{H}_2\text{O}$). They are non-spherical solid particles with threshold formation temperature between 190 and 195 K .

Type Ib PSC

Type Ib PSCs are composed of a supercooled liquid ternary solution of nitric acid, sulfuric acid and water ice ($\text{HNO}_3 \cdot \text{H}_2\text{SO}_4 \cdot \text{H}_2\text{O}$). They also have threshold formation temperature between 190 and 195 K.

Type I PSCs are generally smaller than Type II PSCs, with particle diameters on the order of 1 micron, thereby having a slow sedimentation rate on the order of 0.01 km/day.

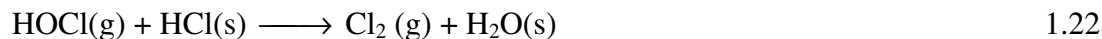
Type II PSC

Type II PSCs are water ice particles (Toon et al., 1989) that form when the temperature falls below 188 K. They are crystalline and non-spherical particles. They are relatively large, with a diameter of about 10 microns, thus, having a rapid sedimentation rate of about 1.5 km/day.

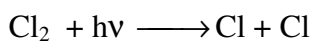
1.4.4 Chlorine Chemistry and Heterogeneous Reactions in the Polar Stratosphere

Heterogeneous reactions are the chemical reactions occurring between gaseous, liquid and/or solid phases. In the stratosphere, they are driven by the occurrence of PSCs that form under very cold winter conditions inside the polar vortex in the northern and southern hemispheres. The PSC particles provide surfaces for heterogeneous reactions to free chlorine and bromine from reservoir species into reactive forms and convert reactive nitrogen species (NO_x) into unreactive, more stable forms such as nitric acid (HNO_3).

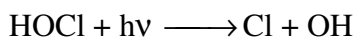
There are 5 basic heterogeneous reactions necessary to understand stratospheric chlorine chemistry, these are:



Equation 1.21 is the most important. HCl and ClONO₂ are mostly unreactive in their solid and gaseous forms respectively. But when they are dissolved in PSCs particles, they become highly reactive with one another leading to reaction 1.21, releasing Cl₂ and retaining HNO₃ with the cloud particles. As soon as the sun reaches the polar vortex, the Cl₂ molecules are photolyzed into two chlorine atoms,

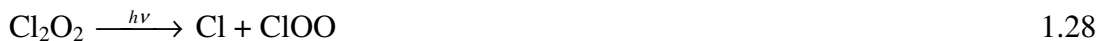


or



and these participate in the reactions leading to two possible catalytic cycles :

1st catalytic cycle



2nd catalytic cycle



or



or



This research work focuses on the 1st catalytic cycle. A schematic diagram illustrating the impact of equation (1.21) and the 1st catalytic cycle on chemical ozone destruction is shown in figure (1.4).

It should be observed that there are no O atoms involved in these catalytic cycles, still reactive chlorine is produced when ClO dimer (Cl_2O_2) is photolyzed by ultraviolet light.

As shown in

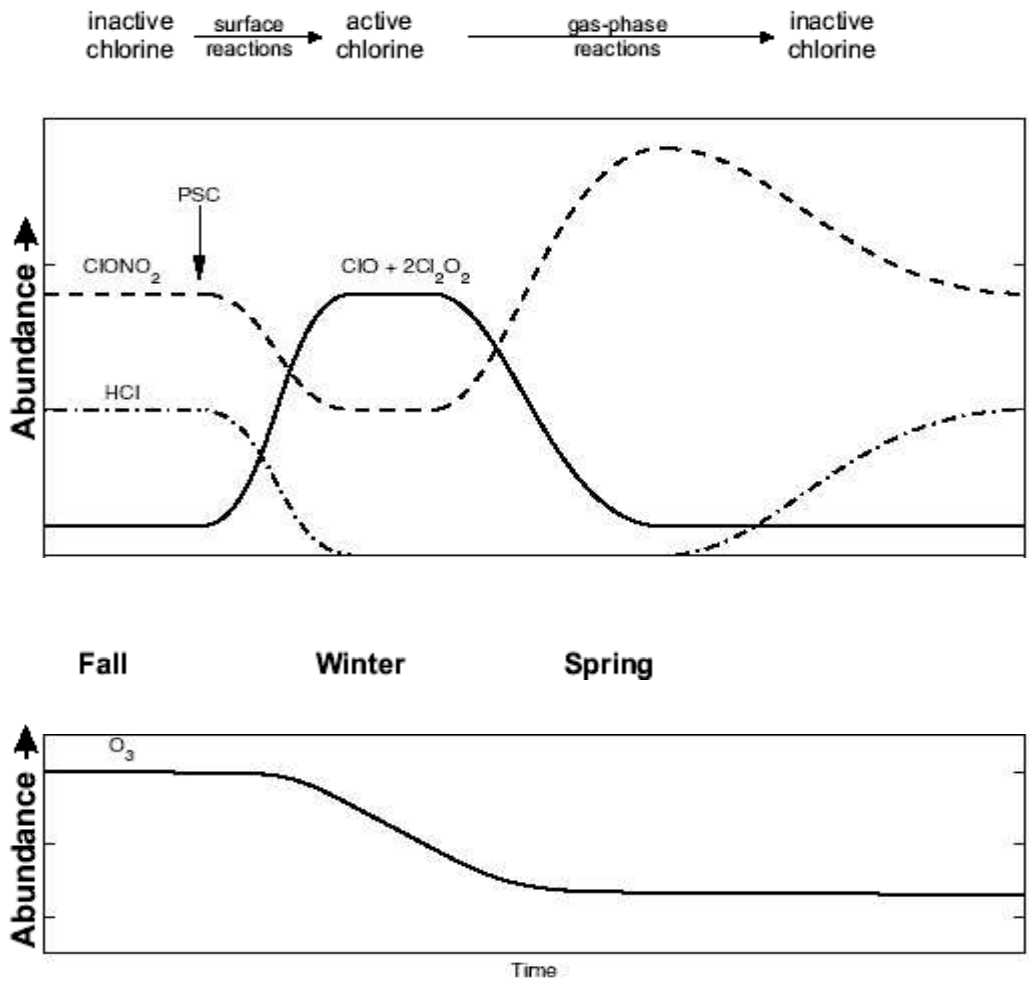


Figure 1.4: Schematic diagram of the reactions between the chlorine reservoir species HCl and ClONO₂ with corresponding ozone destruction (adapted from B-M Sinnhuber)

figure 1.5 the rate limiting reaction to 1st catalytic cycle is the reaction between ClO and NO₂ as given below:



This is a deactivation reaction that takes place at the end of polar winter, when sunlight comes back to the polar regions, provided there is no denitrification (denitrification is explained in the next section). Equation (1.36) is an important link between chlorine chemistry and

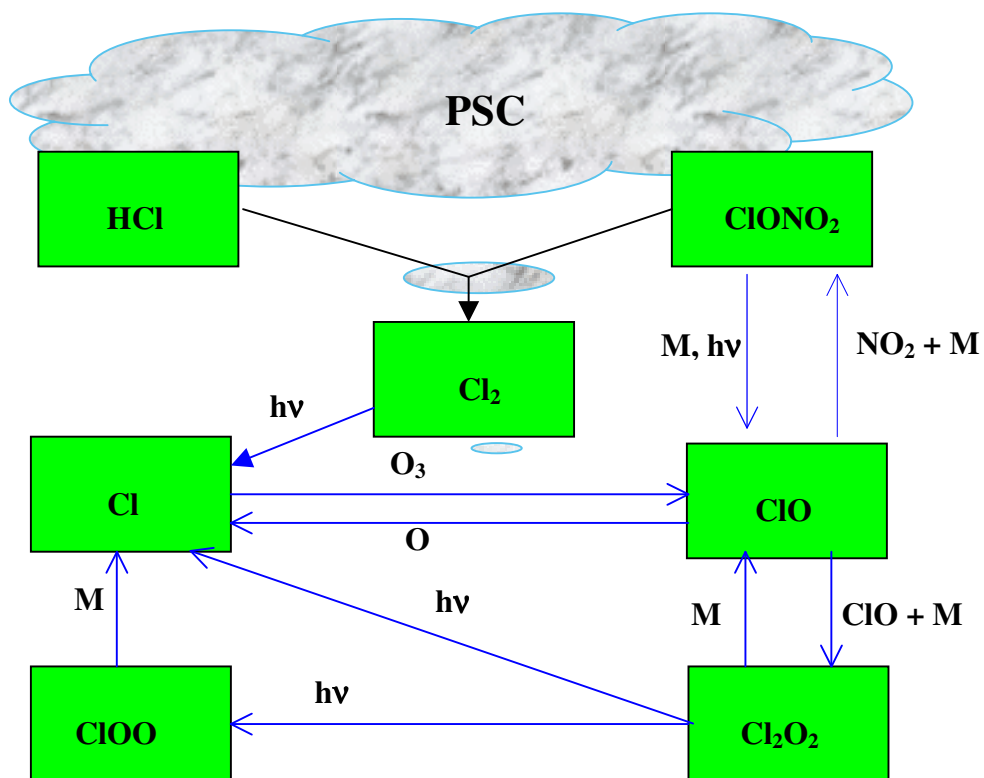


Figure 1.5: A schematic diagram showing simplified form of relevant reactions during activation and deactivation of chlorine, with subsequent loss of ozone. $h\nu$ refers to sunlight

nitrogen chemistry in the polar stratosphere. The NO_2 is from photolysis of HNO_3 as shown in equation (1.37):



1.4.5 Denitrification

Denitrification is the irreversible removal of reactive nitrogen from the polar stratosphere by the sedimentation of particles containing HNO_3 (Kleinböhl, 2003). The unreactive HNO_3 formed in reaction 1.21 remains in a solid state on the surfaces of the PSCs. As the PSCs undergo sedimentation, the HNO_3 is carried out of the stratosphere. This process leads to the reduction in the amount of reactive NO_2 released by photolysis of HNO_3 in polar spring in the stratosphere, since HNO_3 photolysis results in the formation of reactive NO_2 . Thus, the resultant effect of denitrification is the retardation of chlorine deactivation which implies prolonged ozone destruction.

2. Microwave Measurement Techniques

By detecting microwave radiation, with wavelengths from about 0.1mm to a few tens of centimeters, observation during any time of the day is possible without restriction. This is an advantage over other remote sensing techniques. There are two types of microwave remote sensing; active and passive. The active type receives the backscattering that is reflected from the transmitted microwave which is incident on the ground surface. A good example is the RADAR. The passive type detects thermal emission from the target. The Airborne Submillimeter Radiometer ASUR instrument is an example of a passive microwave sensor.

2.1 Radiative transfer

Radiative transfer is the process of transmission of the electromagnetic radiation through the atmosphere. This process is characterized by absorption, emission, and scattering. Both absorption and scattering are referred to as extinction processes since they involve reduction in the intensity of solar radiation. In ASUR measurements, Rayleigh scattering with air molecules can be neglected, since the instrument operates at submillimeter wavelengths. In addition, scattering at cloud particles can be neglected since the

instrument measures on board an aircraft flying above the troposphere where presence of clouds is not expected except for cirrus and polar stratospheric clouds whose particles are assumed to be smaller ($1\mu\text{m}$) than the wavelength of the radiation ($500\mu\text{m}$).

2.1.1 Radiative transfer Equation

The radiative transfer equation shall only be based on absorption and emission and since these processes are linear, they are additive. Therefore, as absorption and emission are the only two processes that modify the intensity of radiation, the radiative transfer equation can be written as:

$$\frac{dI}{ds} = -\alpha_\nu I_\nu + S_\nu \quad 2.1$$

I_ν is the intensity of the radiation at a given frequency, s is the path in the air, α_ν is the absorption coefficient of the atmosphere, and S_ν is the source term for the thermal emission. Noting that in terms of molecular spectroscopy, local thermal equilibrium indicates that energy levels of any medium are populated according to Maxwell/Boltzmann statistics. This can be assumed if the following are valid:

- i. $h\nu \ll K_B T$

i.e the photon energy is much less than the kinetic energy of the molecule; although this breaks down for extremely high frequencies or low temperatures.

ii. rate of collision high enough; this breaks down at very low pressure

iii. intensity not too large.

For lines at submillimeter wavelengths, local thermal equilibrium can be assumed throughout the stratosphere; thereby the source term of the radiation can be represented by the product of Planck's function, which describes the black body radiation, and the absorption coefficient. A black body is an object with uniform temperature and an emissivity equal to 1 i.e. no reflection. Planck's law describes the black body radiation as given below:

$$B(\nu, T) = \frac{2h\nu^3}{c^2} \frac{1}{e^{h\nu/KT} - 1} \quad 2.2$$

with $B(\nu, T)$ the Planck's function, h is Planck's constant 6.63×10^{-34} J s, ν is the frequency of the radiation, c is the speed of light, 3.0×10^9 ms⁻¹, k is Boltzmann constant 1.38×10^{-23} J K⁻¹ and T is the temperature of the object.

Thus we have,

$$S_\nu = \alpha_\nu B(\nu, T) \quad 2.3$$

i.e

$$S_\nu = \frac{2h\nu^3}{c^2} \frac{\alpha_\nu}{e^{h\nu/KT} - 1} \quad 2.4$$

Substituting eq. 2.3 to eq. 2.1 and solve analytically by integration, the intensity at an altitude h is given by

$$I_\nu = I_0 e^{-\tau_\nu(h, \infty)} + \int_h^\infty \alpha_\nu B(\nu, T) e^{-\tau_\nu(h, s)} ds \quad 2.5$$

This is the integral form of the scalar radiative transfer equation. I_0 is the background radiation, τ_ν is the optical thickness between the altitudes h and s. It gives the amount of extinction a beam of light experiences while traveling between two points. The optical thickness is expressed as;

$$\tau(s, s') = \int_s^{s'} \alpha_\nu(s') ds' \quad 2.6$$

2.1.2 BRIGHTNESS TEMPERATURE

Brightness temperature is the temperature that a blackbody would need to have in order to emit radiation of the observed intensity at a given wavelength. This can be derived from eq. 2.7:

$$I(\nu, T) = \varepsilon(\nu)B(\nu, T) \quad 2.7$$

Using eq 2.2 and noting that emissivity of a black body is 1, eq. 2.7 becomes:

$$I(\nu, T) = \frac{2h\nu^3}{c^2} \frac{1}{e^{h\nu/K_B T} - 1} \quad 2.8$$

In general, radiation intensity at submillimeter wavelengths is expressed as brightness temperature that can be obtained from eq. 2.8 giving

$$T_{PLANCK} = \frac{h\nu}{k_B \ln\left(\frac{2h\nu^3}{c^2 I}\right)} \quad 2.9$$

Furthermore the temperature from Planck's equation can be replaced by the Rayleigh-Jeans approximation, obtained by doing a Taylor series expansion of the exponential in the Planck's function, giving

$$\exp\left(\frac{h\nu}{k_B T}\right) \approx 1 + \frac{h\nu}{k_B T} \quad 2.10$$

Substituting eq 2.10 into eq.2.8, we have

$$T_{RJ} = \frac{c^2}{2\nu^2 k_B} I_\nu \quad 2.11$$

However, this approximation is valid only up to frequency of 300GHz i.e not in submillimeter wavelength range.

2.2 Line Broadening and Intensity

Thermal emissions lead to transitions between discrete energy states in a gas molecule.

These transitions result in spectral lines and intensities as described in next subsections.

2.2.1 Line shape

Three primary processes determine the observed shape of spectral lines. These are the natural line width, pressure broadening and Doppler broadening. The Natural line width, which originates from the Heisenberg uncertainty principle, is negligible in the atmosphere, where only pressure- and doppler-broadening effects dominated line shapes.

Doppler broadening is intermediate in importance between natural line shape and

pressure broadening. At pressures lower than about 1 mb, collisions become small enough that the line shapes change from Lorentzian to Doppler, where it becomes a convolution of Lorentzian and Doppler shapes. This convolution is known as the Voigt line shape.

Natural line width

As indicated above, this is a consequence of Heisenberg's uncertainty principle that may be expressed as the fundamental uncertainty relating two conjugate coordinates such as position and momentum, or, in this case, time and energy. Radiative transitions from an upper to a lower state may occur spontaneously. The time intervals t between spontaneous emission are described by a Poisson distribution

$$p(t) = \frac{1}{\tau} e^{-t/\tau} \quad 2.12$$

where τ is the mean lifetime of the excited state.

However, the time-dependent Schroedinger equation predicts that the relation between the time intervals between such decays and the energy of the decays gives rise to a continuous profile of absorption and emission. The resulting profile is called the natural line shape and is described by Lorentz line shape given as

$$F_N(\nu, \nu_{if}) = \frac{\gamma_N}{\pi} \frac{1}{(\nu - \nu_{if})^2 + \gamma_N^2} \quad 2.13$$

where γ_N is the natural line shape half width at half-maximum (HWHM).

The limited lifetime leads to an uncertainty in the energy ΔE of the transition giving

$$\tau \cdot \Delta E = \frac{\hbar}{2} \quad 2.14$$

A typical value of τ is 10^8 s. This is an extremely long time relative to the typical mean time between collisions in the stratosphere and mesosphere, order 10^{-10} s. Thus, the natural line width is negligible for submillimeter spectroscopy in the stratosphere.

Pressure Broadening

This is a result of collisions between molecules and it is the most important cause of line broadening in the lower atmosphere. It is also called collision broadening. Statistically, collisions in a gas of molecules of uniform velocities take place at random time intervals about a mean value. As with spontaneous decay, the probability distribution of time intervals between collisions is therefore a Poisson distribution as given in eq. 2.12. These collisions reduce the lifetime of an excited state in a molecule and hence lead to an increase of the energy uncertainty of a transition. Pressure broadening is described by a Lorentzian line shape given by:

$$F_c(\nu, \nu_{if}) = \frac{\gamma_c}{\pi} \frac{1}{(\nu - \nu_{if})^2 + \gamma_c^2} \quad 2.15$$

and γ_c is the half width at half-maximum intensity due to pressure (collision) broadening, and it is called the pressure-broadened line width defined as:

$$\gamma_c = \gamma_{c,0} \cdot p \cdot \left(\frac{T_0}{T} \right)^\kappa \quad 2.16$$

where p is the pressure, $\gamma_{c,0}$ is pressure broadening parameter, T_0 is a reference temperature and κ is the line width exponent. Both γ_c and κ are determined experimentally and tabulated in databases such as HITRAN- the ‘high-resolution transmission’ database that provides the parameters required to compute absorption coefficients for all atmospheric transitions of interest. The pressure broadening is dominant in the stratosphere, as can be shown in fig. 2.1. This is used by ASUR instrument to obtain an altitude profile of the mixing ratio of the measured stratospheric constituents.

Doppler Broadening

Brownian motion causes molecules to constantly change their motion relative to the photons which may interact with them. Though the frequencies of resonant absorption are constant in the frame of motion of the molecules, this random thermal movement causes a Doppler shift of the transition frequencies by broadening the range of resonant frequencies in the frame of a stationary observer. This form of line broadening is called

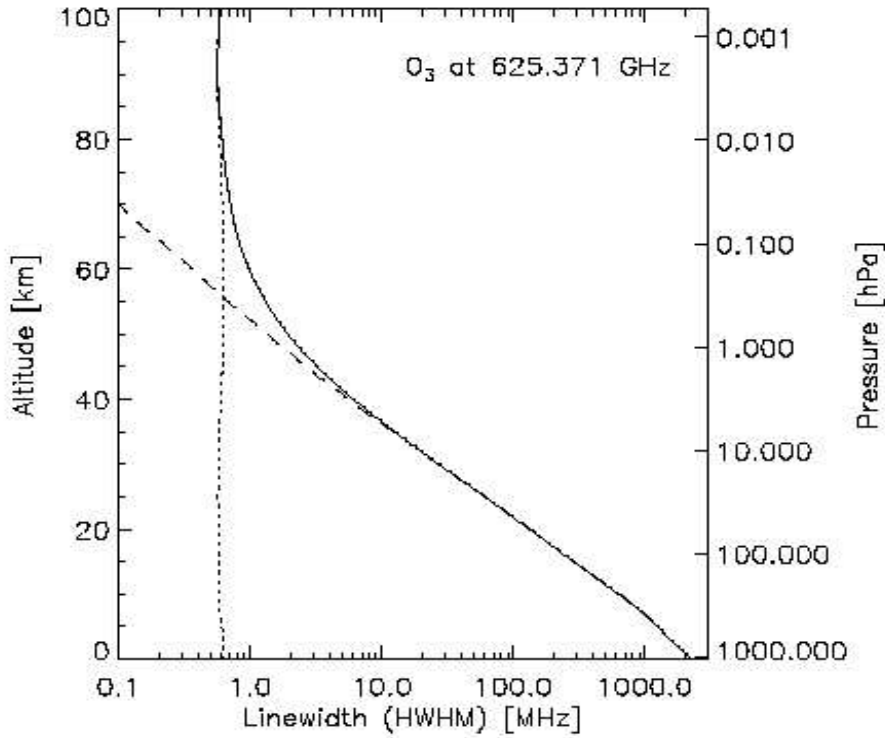


Fig. 2.1 showing linewidths (HWHM) of ozone line at 625.371 GHz for different altitudes in a subarctic winter atmosphere. The Doppler width is shown as a dotted line, the collision induced contribution as a dashed line. The resulting total line width is shown as the solid line. (Kleinböhl A., 2003)

Doppler broadening. The resulting line shape function follows a Gaussian distribution

given by :

$$F_D(\nu, \nu_{if}) = \frac{1}{\gamma_D \sqrt{\pi}} e^{-\left(\frac{\nu - \nu_{if}}{\gamma_D}\right)^2} \quad 2.17$$

γ_D is the Doppler line width (HWHM) described as

$$\gamma_D = \frac{\nu_{if}}{c} \sqrt{\frac{2kT}{m}} \quad 2.18$$

where m is the mass of the molecule.

From figrad1, it can be seen that the Doppler broadening becomes important in the mesosphere.

2.2.2 Line strength

As described by Rosenkranz (1993), the line strength S_{if} of a transition from an initial state i to a final state f is given as:

$$S_{if}(T) \approx \nu_{if} \frac{g_i}{Q(T)} e^{-E_i/kT} \left(1 - e^{-h\nu_{if}/kT}\right) |\mu_{fi}|^2 \quad 2.19$$

This assumes a Maxwell-Boltzmann distribution of state occupation probabilities i.e a local thermal equilibrium. In eq. 2.19, ν_{if} is the frequency of the transition from initial to final state, $|\mu_{fi}|^2$ is the dipole matrix element of the transition, g_i is the statistical weight of the initial state, E_i is the energy of the initial state and $Q(T)$ is the partition function which gives the distribution of energy states of the gas molecules at a particular temperature. Also referred to as line intensities, the line strengths at a reference temperature $S_{if}(T)$, the transition frequencies ν_{if} , the lower state energies E_i and the partition functions $Q(T)$ can be found in data bases e.g HITRAN catalogue (Rothmann, 1992) and JPL catalogue (Pickett, 1998).

2.2.3 Absorption Coefficient

This is the fundamental property of a discrete line transition. It gives the strength of the transition as a function of frequency or wavelength. The absorption coefficients determine the information on the state of the atmosphere. It can be written as

$$\alpha(\nu) = n.S(T).F(\nu) \quad 2.20$$

where $S(T)$ is the line intensity, n is the number density of the absorber and $F(\nu)$ is the normalized line shape function given as :

$$\int F(\nu)d\nu = 1 \quad 2.21$$

2.2.4 Continuum Absorptions

This is a non-resonant absorption that gives rise to the discrepancy between calculated and measured line spectra. Continuum absorption has no spectral features but it increases with frequency and can be divided into water vapor continuum which depends quadratically on water vapor partial pressure, and dry air continuum that depends on total pressure and temperature. A more detailed general idea about continuum models can be found in Buehler (1999) and specifically to ASUR instrument in Kaviani (2003).

2.3 The Airborne Submillimeter Radiometer

The Airborne Submillimeter Radiometer, ASUR (Crewell et al., 1994; Wehr et al., 1995; Küllmann et al., 1999; von König et al., 2000) is a passive heterodyne radiometer operating at frequencies between 604.3 and 662.3 GHz, equivalent to wavelengths between 0.45 and 0.5 mm. It detects thermal emissions from rotational lines of constituents related to stratospheric chemistry and dynamics such as ClO, HCl, N₂O, HNO₃, CH₃Cl, H₂O, HO₂, BrO, HOCl, HCN, NO and ozone. At the frequency range of ASUR, ground-based observations are not practicable due to the strong signal absorption by tropospheric water vapor. The instrument is operated on board of an aircraft flying at an altitude of 10-12 km, such that a major part of the water vapor absorption is avoided. The pressure broadening of the detected emission lines provides vertical profiles from 15 to 70 km altitude, with a vertical resolution of about 6 km and 12 km in the lower and upper stratosphere, respectively. The horizontal resolution is between 12 and 50 km depending on the necessary integration time required to obtain a sufficient signal-to-noise ratio, and the speed of the aircraft. The instrument was developed at the University of Bremen in 1991 under the name Submillimeter Atmospheric Sounder, SUMAS. An implementation of a helium-cooled superconducting detector in co-operation with the Space Research Organization of the Netherlands (SRON) was carried out in 1994, and several other improvements have been undertaken on the instrument in following years,

e.g the frequency range has been extended to measure new species. These improvements have considerably reduced the system noise temperature, and hence increase the spatial and temporal resolution of the instrument.

2.3.1 Heterodyne Principle

Broadly, the heterodyne principle entails the generation of new frequencies by mixing two or more signals in a nonlinear device such as a transistor or diode mixer. Since the frequency range of ASUR instrument is too large for a direct conventional electronic amplification, this heterodyne method is applied in its operation. It converts the signal to a lower frequency range without changing the spectral information of the signal. The cutback in frequency permits the use of conventional electronic amplifiers with subsequent filtering and detection of the signal. This method gives good spectral resolutions and high signal-to-noise ratios. The principle uses an artificial signal of a local oscillator (LO) and heterodynes it with the atmospheric signal. A mixer, which is a superconducting diode with non-linear current-voltage characteristic, is then used to convert these signals to the intermediate frequencies. This principle can be mathematically represented by doing a Taylor series expansion of the current that goes into the mixer. Because of the non-linearity of the mixer, the current is given as:

$$I(U_0 + \delta U) = k_0 + k_1 \delta U + k_2 \delta U^2 + k_3 \delta U^3 + \dots \dots \dots \quad 2.22$$

neglecting higher order.

Assuming the signal frequency ν_s and local oscillator ν_{LO} are monochromatic with

$$\delta U = A \sin \omega_{LO} t + B \sin \omega_s t \quad 2.23$$

where $\omega_{LO} = 2\pi\nu_{LO}$ and $\omega_s = 2\pi\nu_s$ are the angular frequencies, eq. 2.22 becomes:

$$\begin{aligned}
 I = & k_0 + k_1 (A \sin \omega_{LO} t + B \sin \omega_s t) \\
 & + k_2 \left(\frac{A^2}{2} + \frac{B^2}{2} \right) \quad \text{DC term} \\
 & - k_2 \left(\frac{A^2}{2} \cos(2\omega_{LO} t) + \frac{B^2}{2} \cos(2\omega_s t) \right) \quad \text{Higher harmonics} \\
 & + k_2 (AB(\cos(\omega_{LO} - \omega_s) t)) \quad \text{Difference frequencies (Intermediate frequency)} \\
 & - k_2 (\cos(\omega_{LO} + \omega_s) t) \quad \text{Sum frequencies}
 \end{aligned}$$

2.24

The sum frequencies, higher harmonics and other products of the mixing process are suppressed using appropriate bandpass filters. In general, the intermediate frequency contains contributions of the lower sideband (lsb) and the upper sideband (usb) of the receiver. If the receiver is sensitive to both sidebands at the same time, it works in double sideband (DSB) mode. If one of the sidebands is significantly suppressed by interferometers, the receiver works in single sideband (SSB) mode. The sideband where the signal is located is called the signal band and the other is called image band.

Additional mixing stages are applied followed by corresponding bandpass filtering, conventional amplification, insulation and attenuation. However, since only the first components of a radiometer contribute significantly to the noise of the radiometer (Vowinkel, 1988), in order to reduce radiometric noise, it is sufficient to cool the first mixer stage and the first amplifier of ASUR instrument.

2.3.2 Calibration

The radiometric signal has to be calibrated in order to obtain the atmospheric signal since the detected power P has contributions from both atmospheric radiation $P_{\text{atmosphere}}$ and radiometric noise P_{system} . Because we can relate the atmospheric radiated power with brightness temperature of an object, the calibration is done by measuring calibration loads that can be considered as black bodies at different temperatures. Recall the Planck's function for a black body (eq. 2.2):

$$B(\nu, T) = \frac{2h\nu^3}{c^2} \frac{1}{e^{h\nu/KT} - 1}$$

As indicated earlier,

$$P = P_{\text{atmosphere}} + P_{\text{system}} \tag{2.25}$$

And on assumption of a linear relationship between the temperature and radiated power of an object, we have

$$P_{\text{atmosphere}} = GT_{\text{atmosphere}} \quad 2.26$$

G is an amplification factor called the pre-detection gain. Putting eq. 2.26 into 2.25, it implies that

$$P = GT_{\text{atmosphere}} + P_{\text{system}} \quad 2.27$$

G and P_{system} can then be derived from the calibration measurements by the expressions

$$G = \frac{P_{\text{hot}} - P_{\text{cold}}}{T_{\text{hot}} - T_{\text{cold}}} \quad 2.28$$

and

$$P_{\text{system}} = P_{\text{cold}} - GT_{\text{cold}} \quad 2.29$$

By substituting eqs 2.28 and 2.29 into eq 2.27, we have

$$T_{\text{atmosphere}} = \frac{T_{\text{hot}} - T_{\text{cold}}}{P_{\text{hot}} - P_{\text{cold}}} (P - P_{\text{cold}}) + T_{\text{cold}} \quad 2.30$$

which gives the radiated power of the atmosphere expressed as temperature.

Similarly by plotting eq. 2.27 and extrapolating the graph, then define the system noise temperature as a virtual point where no power is detected, we have

$$T_{\text{system}} = \frac{T_{\text{hot}} - T_{\text{cold}}}{P_{\text{hot}} - P_{\text{cold}}} P_{\text{cold}} - T_{\text{cold}} \quad 2.31$$

Eq. 2.31 gives the radiometric noise expressed as temperature, and the graph is indicated as in fig 2.2.

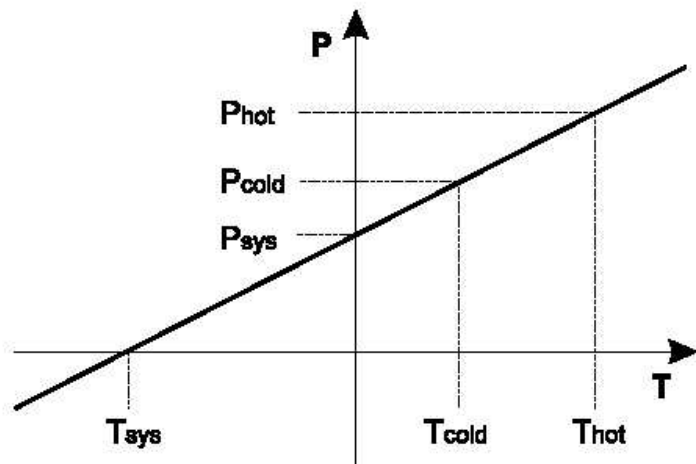


Fig 2.2: Figure showing the method used in ASUR instrument's calibration

2.3.3 Instrumental assembly

The ASUR instrument is made up of two racks, a frontend and a backend rack. The racks are mounted inside the aircraft cabin using rubber shock mounts in order to protect the instrument from shocks and vibrations.

Frontend

The frontend rack contains the calibration unit, quasi-optical system, mixer, and the intermediate frequency chain. The microwave radiation enters the aircraft through a high density polyethylene (HDPE) window, after which it is collected by a rotatable mirror. The mirror is controlled to compensate for the aircraft roll angle such that all atmospheric

measurements are performed at the same elevation angle. For ASUR measurements, an elevation angle of 12° is used. The mirror switches between the atmospheric signal and two calibration signals (cold and hot loads), and reflects them into the quasi-optical system, schematically shown in 2.3. The mirror points in regular intervals of two seconds at the hot and cold calibration loads. The calibration loads are black body emitters. The hot load is at ambient temperature of the aircraft while the cold load is liquid nitrogen with a temperature of 77 K. The quasi-optical system is made up of a pathlength modulator and two Martin-Puplett-interferometers . The pathlength modulator is used to reduce standing waves. The first interferometer is used to suppress any unwanted side band while the other is used as a diplexer to combine the atmospheric and the local oscillator signals, and finally injects them into the mixer.

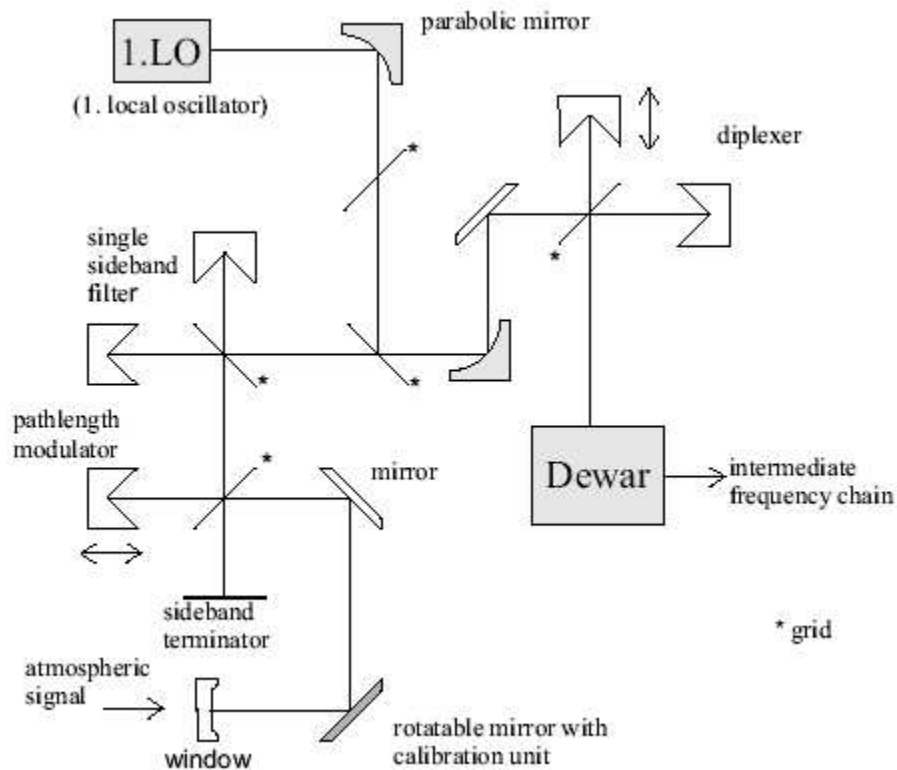


Fig 2.3. Schematic showing the quasi-optical system of ASUR instrument, courtesy Bremer, 2002

After leaving the quasi-optical system, the signal is received by the detector that is located inside a dewar filled with liquid helium and liquid nitrogen. The detector is made up of a superconductor-insulator-superconductor (SIS) junction that gives rise to low system noise temperatures. Depending on the measured frequency, noise temperature between 550 and 1450 K in single sideband mode can be achieved. Inside the dewar, liquid nitrogen is used as a heat buffer between the liquid helium temperature and the ambient temperature of the aircraft. The heterodyned signal is then amplified and filtered.

The first amplifier is a high electron mobility transistor [HEMT] cooled with liquid helium so as to guarantee a low system noise temperature of the radiometer. After the first mixing and amplification processes, the signals have a frequency of (11.4 ± 2.25) GHz. In two following mixing steps they are transformed to the input frequencies of the two spectrometers. These are (2.3 ± 0.75) GHz and (1.35 ± 0.09) GHz for AOS and CTS respectively. The steps involved in the signal processing are shown in 2.4.

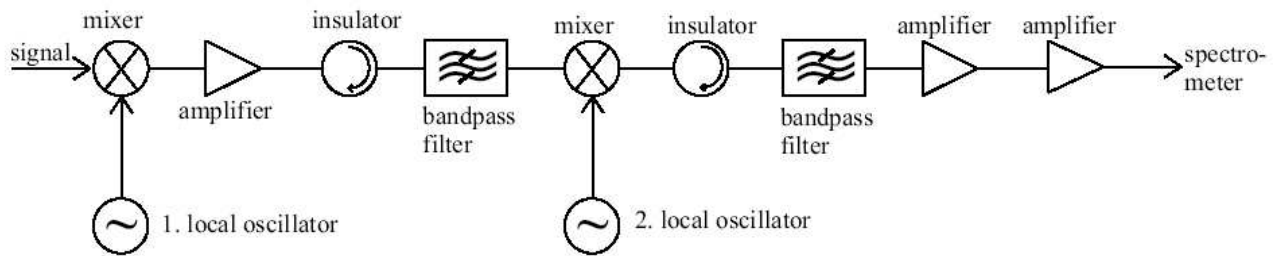


Figure 2.4 showing the signal processing steps of ASUR instrument. Bremer, 2002

Backend

The backend rack contains the spectrometers and a computer used for experimental control, data acquisition and storage. The spectrometers used in ASUR instrument are described in next subsection. The computer also reads out and stores information on altitude and geographical location and other data provided by the on-board computer of the aircraft. The spectrometers analyze and digitize the signals while the computer reads out the spectral information.

2.3.4 Spectrometers

The development of heterodyne receivers in atmospheric research and other applications have prompted a high demand for wide bandwidth and/or multi-band back-ends. Predominantly in the sub-millimeter range, the request for large bandwidth poses a challenge for the development of suitable back-ends. The ASUR instrument depends crucially on versatile back-end in order to achieve a most economic usage of the available equipment with maximum scientific return. There are two types of spectrometers used in ASUR instrument. These are the acousto-optical spectrometer (AOS) and the chirp-transform spectrometer (CTS).

Acousto-Optical Spectrometer

In ASUR's acousto-optical spectrometer, the intermediate frequency is coupled to a Bragg cell through a piezoelectric transducer made up of a quartz crystal. The signal generates mechanical oscillations in the crystal and this produces density variations with subsequent change in the refractive index of the Bragg cell. A laser illuminates the Bragg cell. The cell refracts the monochromatic light from the laser beam and the signal is then focused onto a CCD line detector containing 1728 useable channels. Thereafter the signal is digitally converted and fed to a computer system. Each channel has a width of 0.89 MHz, bandwidth of 1.5 GHz and a resolution of 1.5 MHz.

Chirp-Transform Spectrometer

In CTS, the signal is modulated with a Chirp i.e linear shift in frequency, thereby a fixed frequency signal becomes a linearly changing frequency. The new signal is led into a dispersive filter with a delay time depending on frequency. The filter output for the fixed frequency is now a single pick at a specific time giving the spectrum as a function of time. The main feature of ASUR's chirp-transform spectrometer is its high frequency resolution of 278 kHz. It has 638 usable channels and covers a bandwidth of 178 MHz. The center frequency of the CTS can be adjusted to other spectral lines, and it is not affected by fluctuations in temperature. These cannot be accomplished by the AOS. An introduction to chirp-transform spectrometry can be found in Hartogh, 1989. With implementation of the CTS to ASUR instrument, the altitude range has been extended up to the mesosphere.

3. RETRIEVAL AND ANALYSIS OF DATA

The retrieval of atmospheric parameters from remote sensing data requires accurate calculations that determine the received microwave radiation for specific atmospheric conditions, since the sensor measures complicated functions of the quantities of interest. These measurements do not give the actual state of the atmosphere with independent errors, but only the best estimate derivable from the measurements and prior knowledge about the state of the atmosphere. Thus, the intensity and spectral distribution can be calculated given the profiles of the constituents in the atmosphere and relationship between altitude, pressure and temperature.

3.1 Optimal estimation Method

The Optimal estimation method (Rodgers 1976, 1990, 2000) describes the relationship between the remote measurements and the true atmospheric state, with an extensive analysis of errors involved. It is a special case of model fitting that minimizes the difference between model prediction and measurement, by adjusting fit parameters.

The mathematical representation of quantities measured in any remote sensing is given by:

$$\mathbf{y} = F(\mathbf{x}, \mathbf{b}) + \boldsymbol{\varepsilon} \tag{3.1}$$

where \mathbf{y} is the vector of the measured intensities for certain frequencies, \mathbf{x} the vector of the intended constituent profiles, \mathbf{b} a set of model parameters comprising quantities that influence the measurements and are known to some accuracy, e.g. the relationship between altitude, pressure and temperature, $\boldsymbol{\varepsilon}$ the experimental error contribution and F the forward model that describes the radiative transfer given by equation 2.5.

However, equation 3.1 cannot be directly implemented in remote sensing, since a set of constituent profiles has to be retrieved from a measured intensity distribution. Thus, equation 3.1 is reversed and the process is termed inversion of the radiative transfer equation. This requires a numerical approach, as there is no analytical solution for the inversion of equation 2.5. By using a χ^2 -test cost function, the numerical solution minimizes the difference between a measurement \mathbf{y} and a model calculation $F(\mathbf{x}, \mathbf{b})$. This is given as:

$$\chi_{\boldsymbol{\varepsilon}}^2 = [\mathbf{y} - F(\mathbf{x}, \mathbf{b})]^T \mathbf{S}_{\boldsymbol{\varepsilon}}^{-1} [\mathbf{y} - F(\mathbf{x}, \mathbf{b})] \quad 3.2$$

where $\mathbf{S}_{\boldsymbol{\varepsilon}}$ is the covariance matrix. It gives the errors and their correlation with the measurement vector \mathbf{y} .

However, it is necessary to use additional apriori information about the state of the atmosphere in order to constrain the retrieval. This can be a climatology derived from

a set of independent measurements of the atmospheric constituents to be retrieved. It is important because several atmospheric states \mathbf{x} may exist that satisfy equation 3.1 for a measured radiation distribution \mathbf{y} , leading to finite measurements for continuous unknowns. This makes the inversion ill-conditioned. Similarly, noise amplification can be prevented by constraining the retrieval since small errors in the measured quantity \mathbf{y} leads to large errors in the retrieved quantity \mathbf{x} . The additional information leads to a second χ^2 -test as given below:

$$\chi_{\varepsilon}^2 = [\mathbf{x} - \mathbf{x}_a]^T \mathbf{S}_a^{-1} [\mathbf{x} - \mathbf{x}_a] \quad 3.3$$

where \mathbf{x}_a is the vector containing the apriori information and \mathbf{S}_a is the apriori covariance matrix taken from the climatology.

Finally, the difference between the state vector of the atmosphere and the apriori vector is also minimized by adding their cost functions:

$$\chi^2 = \chi_{\varepsilon}^2 + \chi_a^2 \quad 3.4$$

i.e.

$$\chi^2 = [\mathbf{y} - F(\mathbf{x})]^T \mathbf{S}_{\varepsilon}^{-1} [\mathbf{y} - F(\mathbf{x})] + [\mathbf{x} - \mathbf{x}_a]^T \mathbf{S}_a^{-1} [\mathbf{x} - \mathbf{x}_a] \quad 3.5$$

Eq. 3.5 is the fundamental equation for the optimal estimation method (OEM). The minimum of the cost function is found depending on the non-linearity of the forward model. For an optically thin atmosphere, i.e. atmosphere whose optical thickness approximately equals to zero, the forward model in eq 3.1 can be replaced with a matrix so that the inversion can be done with simple matrix algebra. This is a totally linear case. But since such assumption is not applicable in the context of this research work, a Taylor series expansion is used to linearly approximate the forward model around a reference state \mathbf{x}_0 so that eq. 3.1 becomes:

$$\mathbf{y} = F(\mathbf{x}_0, \mathbf{b}) + \mathbf{K} \cdot (\mathbf{x} - \mathbf{x}_0) + \varepsilon \quad 3.6$$

where \mathbf{K} is the weighting function matrix given as :

$$\mathbf{K} = \left. \frac{\partial F(\mathbf{x}, \mathbf{b})}{\partial \mathbf{x}} \right|_{\mathbf{x}_0} \quad 3.7$$

Eq. 3.7 is calculated analytically in order to save computer time.

For a forward model that is strongly non-linear, sophisticated iteration schemes like the Levenberg-Marquardt method (Press et al., 1992) or Monte Carlo technique can be used. But for ASUR retrieval whose forward model is weakly non-linear, since the high water vapor concentration of the troposphere is avoided, a simple Newton iteration scheme

(Press et al., 1992) is used in addition to linearization of the forward model. The state vector is then given by:

$$\hat{\mathbf{x}}_{n+1} = \hat{\mathbf{x}}_n + \left(\mathbf{S}_a^{-1} + \mathbf{K}_n^T \mathbf{S}_\varepsilon^{-1} \mathbf{K}_n \right)^{-1} \cdot \left(\mathbf{K}_n^T \mathbf{S}_\varepsilon^{-1} (\mathbf{y} - F(\hat{\mathbf{x}}_n)) + \mathbf{S}_a^{-1} (\hat{\mathbf{x}}_a - \hat{\mathbf{x}}_n) \right) \quad 3.8$$

$\hat{\mathbf{x}}_{n+1}$ is the retrieved state vector of the (n+1)th iteration step.

A fixed number of iterations is chosen above which the retrieval of an atmospheric constituent does not improve anymore. A convergence criterion can also be defined.

3.2 Analysis of Retrieval Errors and Altitude Resolution

The retrieval method R of the retrieved parameters of equation 3.1 can be described by:

$$\hat{\mathbf{x}} = R(\mathbf{y}, \hat{\mathbf{b}}, \mathbf{x}_a) \quad 3.9$$

where $\hat{\mathbf{x}}$ is the retrieved state vector, \mathbf{y} the measurement vector and $\hat{\mathbf{b}}$ the best estimate of the forward model parameters. Putting equation 3.1 into equation 3.9, we have:

$$\hat{\mathbf{x}} = R\left(F(\mathbf{x}, \mathbf{b}) + \varepsilon, \hat{\mathbf{b}}, \mathbf{x}_a\right) \quad 3.10$$

The forward model F is linearized about $\mathbf{x} = \mathbf{x}_a$ and $\mathbf{b} = \hat{\mathbf{b}}$, while the retrieval method R is linearized about $\mathbf{y} = F(\mathbf{x}_a, \hat{\mathbf{b}})$. This leads to the following Jacobi matrices:

$$\mathbf{K}_x = \left. \frac{\partial F(\mathbf{x}, \mathbf{b})}{\partial \mathbf{x}} \right|_{\mathbf{x}_a} \quad 3.11$$

$$\mathbf{K}_b = \left. \frac{\partial F(\mathbf{x}, \mathbf{b})}{\partial \mathbf{b}} \right|_{\hat{\mathbf{b}}} \quad 3.12$$

$$\mathbf{G}_y = \left. \frac{\partial R(\mathbf{y}, \hat{\mathbf{b}})}{\partial \mathbf{y}} \right|_{\mathbf{y}=F(\mathbf{x}_a, \hat{\mathbf{b}})} \quad 3.13$$

\mathbf{G}_y is the contribution function matrix. Putting these matrices into equation 3.10, we have:

$$\begin{aligned} \hat{\mathbf{x}} = & \underbrace{R(F(\mathbf{x}_a, \hat{\mathbf{b}}), \hat{\mathbf{b}}, \mathbf{x}_a)}_{\text{BIAS}} \\ & + \underbrace{\mathbf{G}_y \mathbf{K}_x (\mathbf{x} - \mathbf{x}_a)}_{\text{SMOOTHING}} \\ & + \underbrace{\mathbf{G}_y \mathbf{K}_b (\mathbf{b} - \hat{\mathbf{b}})}_{\text{MODEL PARAMETER}} \\ & + \underbrace{\mathbf{G}_y \boldsymbol{\varepsilon}}_{\text{RETRIEVAL}} \end{aligned} \quad 3.14$$

In equation (3.14), the first term on the right hand side, the bias, is the error that occurs when the retrieval of a simulated error-free measurement vector does not yield the

atmospheric state vector that was used in the simulation. This may be caused by an apriori vector that contains features which cannot be resolved by the retrieval. Bias is zero in a good retrieval.

The second term on the right hand side of eq. 3.14 refers to the smoothing of the retrieved state vector with respect to the true state of the atmosphere. It represents the way in which the observing system smoothens the profile. This has an extensive effect for a microwave measurement in uplooking geometry like the ASUR, where the altitude information is exclusively obtained from the pressure broadening and the resulting line shape. The altitude resolution of the measurement is given by the averaging kernel matrix \mathbf{A} that is described by the relation:

$$\mathbf{A} = \mathbf{G}_y \mathbf{K}_x \quad 3.15$$

It plays significant role in the descriptions of the information content, as it describes the subspace of state space in which the retrieval must lie. The rows of the averaging kernel matrix contain functions that peak at an appropriate altitude level. The full width half maximum (FWHM) of these functions is a measure for the altitude resolution of the measurement. The vector area \mathbf{a} of the averaging kernels is a measure of the response of the retrieval to certain parts of the state vector (e. g. altitudes). The area is given by:

$$\mathbf{a} = \mathbf{A}\mathbf{u} \quad 3.16$$

\mathbf{u} is a unit vector.

For a good retrieval, area vector \mathbf{a} should be close to one. This indicates that the retrieval is sensitive to the true profile over the considered altitude range. Any part of the area vector \mathbf{a} with values below 0.5 indicates that the retrieval is dominated by the apriori information in that altitude range. The shape of the averaging kernel function is close to Gaussian in ASUR retrievals.

The third term on the right hand side of equation (3.14) refers to errors related to the model parameters. They could emanate from the altitude-pressure-temperature relation, the viewing angle of the instrument, the line intensity or the pressure broadening coefficient. The covariance matrix of model parameter error \mathbf{S}_m is given by :

$$\mathbf{S}_m = \mathbf{G}_y \mathbf{K}_b \mathbf{S}_b \mathbf{K}_b^T \mathbf{G}_y^T \quad 3.17$$

where \mathbf{S}_b is the error covariance matrix of \mathbf{b} .

The fourth term on the right hand side of equation (3.14) is called the retrieval noise. Its covariance \mathbf{S}_n is given by:

$$\mathbf{S}_n = \mathbf{G}_y \mathbf{S}_\varepsilon \mathbf{G}_y^T \quad 3.18$$

The model parameter error and the retrieval noise are both termed the retrieval errors.

In ASUR measurements, the retrieved state vector is treated as a representation of the true state vector smoothed by the averaging kernel functions. Such representation is applicable in any remote sensing instrument with limited altitude resolution. The smoothed true state vector $\tilde{\mathbf{x}}$ can then be expressed as:

$$\tilde{\mathbf{x}} = \mathbf{A}(\mathbf{x} - \mathbf{x}_a) + \mathbf{x}_a \quad 3.19$$

Subtracting eq. 3.19 from eq. 3.14 gives a retrieval equation with no bias and smoothing error. It is expressed as:

$$\hat{\mathbf{x}} - \tilde{\mathbf{x}} = \mathbf{G}_y \mathbf{K}_b (\mathbf{b} - \hat{\mathbf{b}}) + \mathbf{G}_y \boldsymbol{\varepsilon} \quad 3.20$$

3.3 Retrieval and Analysis of ASUR ClO, HCl and Ozone

The retrieval of ASUR stratospheric trace gases are based on the Optimal Estimation Method (OEM) as described in previous section. This provides atmospheric information from the measured submillimeter spectra in the instrument's frequency range. As this research work focuses on chlorine species, the section is dedicated to ClO, HCl and ozone retrievals. An overview of the measurement campaigns treated for this work is provided in Table 3.1.

Campaign	Date of Campaign (First flight –Last flight)	Number of Flights (excluding test flights)	Aircraft	Region Covered
SESAME III	02.02.1995 - 08.03.1995	20	FALCON	Arctic, Europe
GOME/ERS-2 VALIDATION	22.02.1996 – 06.03.1996	11	FALCON	Arctic, Europe
ILAS/ADEOS	19.02.1997 - 26.02.1997	5	FALCON	Arctic
THESEO/HIMSPEC	22.01.1999 - 08.02.1999	5	FALCON	Arctic, Europe
SOLVE/THESEO 2000	16.11.1999 -15.03.2000	23	DC-8	Arctic
EUPLEX	14.01.2003 - 12.02.2003	9	FALCON	Arctic
SCIA-VALUE Phase II	19.02.2003 - 19.03.2003	15	FALCON	Arctic, Europe, Africa

Table 3.1: Overview of ASUR measurement campaigns considered for this research work.

The profile retrieval is performed on equidistant altitude levels of 2 km spacing. This work used data only from the acousto-optical spectrometer (AOS) as the emphasis is on the lower stratosphere. Since the retrieval requires a diagonal spectrum covariance matrix, the AOS data is binned into 4 MHz wide channels to ensure that the individual channels in the retrieval are not correlated.

The altitude-pressure-temperature relation are obtained from synoptic meteorological data from the European Center for Medium range Weather Forecast (ECMWF) and Data Assimilation Office (DAO).

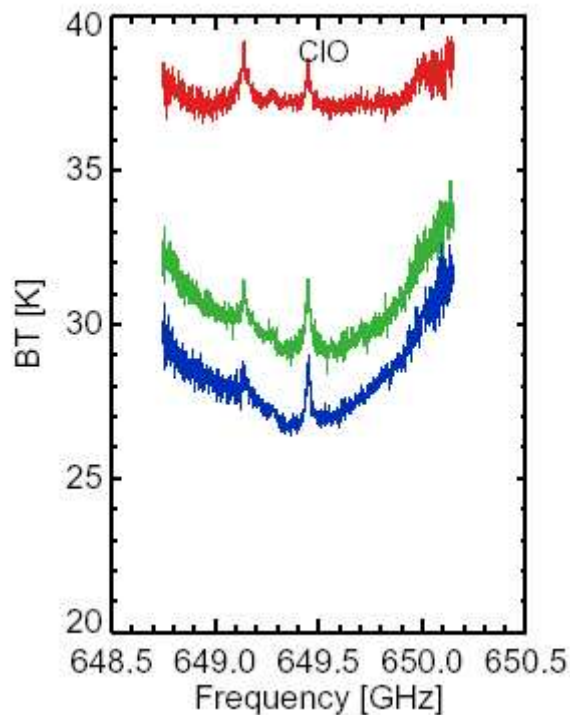


Figure 3.1: Spectra of ClO in tropics, midlatitude and polar region shown by the top, middle and bottom plots respectively. (Courtesy J. Kuttippurath)

For ClO and HCl retrievals, an instrumental center frequency similar to the line frequency is used. A spectral region of ± 600 MHz around the center frequency is then retrieved. However, for ozone retrievals, the frequency band of HCl is used i.e. ozone and HCl are retrieved at the same time from the same measurement. This is because HCl frequency band contains the center of the ozone line as well as a large part of the line wing to higher frequencies. Typical spectra of ClO are given in figure 3.1, while those of HCl and ozone are given in figure 3.2. The three peaks in HCl spectrum is due to its triplet state- a measure of HCl molecular spectroscopy. The frequencies of the measured lines are given in table 3.2, and as can be observed, ozone lines are also present in ClO

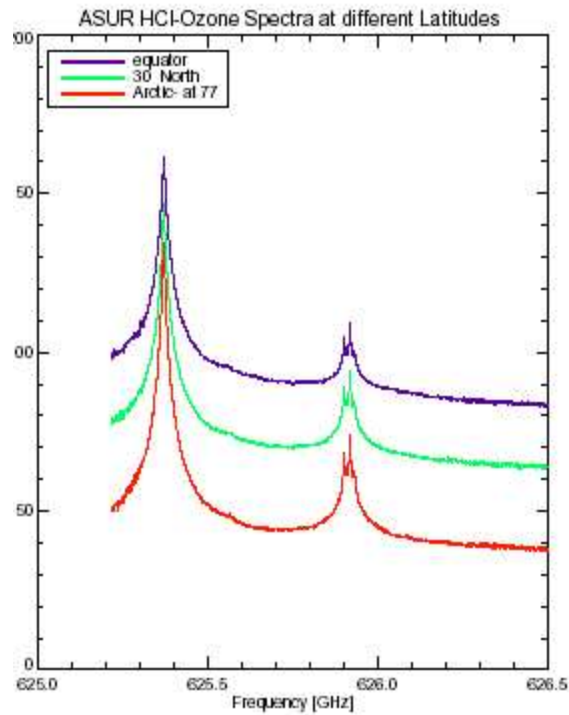


Figure 3.2: Spectra of HCl and ozone in tropics, midlatitude and polar region shown by the top, middle and bottom plots respectively. (Courtesy J.Kuttippurath).

frequency bands. This is the case in all frequency bands of ASUR, although only HCl band gives the best ozone spectral information. Thus ozone/HCl measurements are analyzed first for each flight. The retrieved ozone profiles are interpolated along the flight path and the interpolated profiles are then used as an ozone a priori for the retrieval of ClO. This is also used for other ASUR measured trace gases.

In order to achieve a sufficient signal-to-noise ratio, specific numbers of single spectra are averaged for each of these molecules. This process equally averages out potential errors in the observation angle. The numbers of typically averaged single spectra for ClO, HCl and ozone are also given in Table 3.2. An exemption to these figures was in THESEO/HIMSPEC campaign in 1999, when only 20 and 10 spectra are integrated for ClO and HCl respectively. This was due to shorter measurement time available to the instrument.

Molecule	Line Center Frequency (GHz)	Number of Integrated Spectra	Error from Retrieval Noise (1σ)	Total Retrieval Error	Altitude Range (km)
ClO	649.448	40	≈ 0.06 ppb	$\approx 10\%$, ≥ 0.15 ppb	15 – 43
HCl	625.918	15	≤ 0.08 ppb	$\approx 20\%$, ≥ 0.1 ppb	14 - 51
O ₃	625.371	15	≤ 0.1 ppm	$\leq 15\%$, ≥ 0.6 ppm	14 - 50

Table 3.2: Retrieval features of ClO, HCl and ozone measurements by ASUR. The altitude range of information content is defined as sum of averaging kernels > 0.8 . Compilation from König (2001).

Each spectrum of ASUR measurements corresponds to 2 seconds of observation time in which the instrument's rotating mirror is not corrected for the roll angle of the aircraft. In general, a single measurement takes about 6 seconds in total when calibration measurements and the time required to move the rotating mirror are considered. Thus, a measurement of ClO takes about 4 minutes while HCl and ozone measurements take about 1.5 minutes each.

The horizontal resolution of ASUR measurements is determined by aircraft speed and the integration time required to achieve a sufficient signal-to-noise ratio. Assuming a

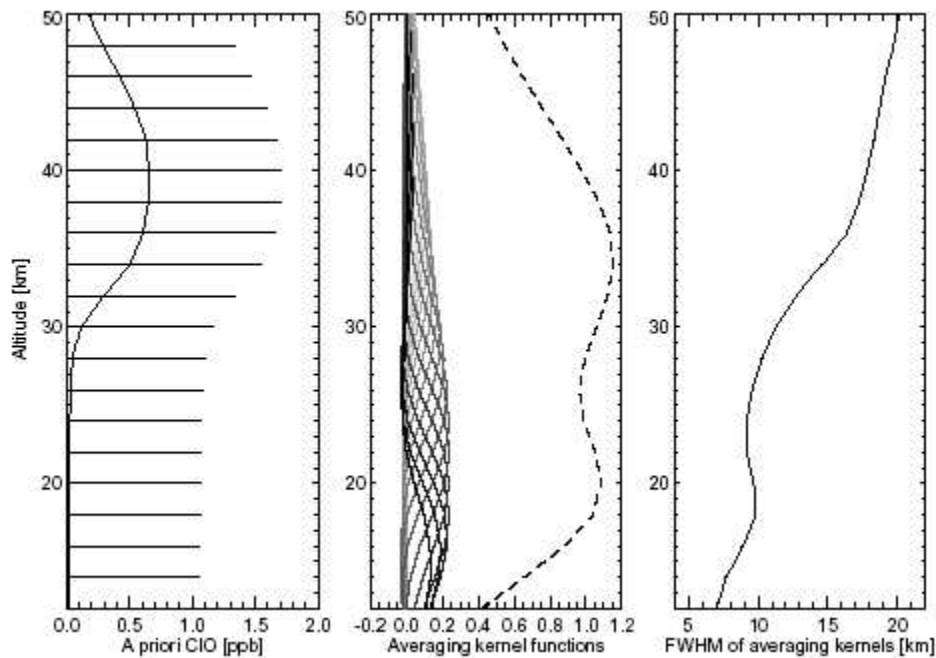


Figure 3.3: Left: A priori profile (solid line) and square root of the a priori covariances (horizontal bars) used for the retrieval of ClO. Middle: Averaging kernel functions (solid lines) and sum of the averaging kernel functions for each altitude level calculated by equation 3.16 (dashed line) for a typical ClO retrieval. Right: Altitude resolution, defined as the FWHM of the averaging kernels at each altitude level, of a typical ClO measurement. (courtesy Kleinböhl, 2003)

nominal aircraft speed of 700 km/h, a horizontal resolution of less than 20 km is achieved for ozone and HCl, while a ClO measurement has about 50 km horizontal resolution. The apriori profiles as well as the square root of the apriori covariance used for these retrievals are given in figures 3.3-3.5 for ClO, HCl and ozone respectively. They are based on climatological values for sub-arctic winter atmospheres.

As noted earlier in previous section, the vertical resolution of ASUR measurements is usually given by the width of their averaging kernel functions. Also shown in figures 3.3-3.5 are the shapes and width of the averaging kernels for ASUR's ClO, HCl and ozone respectively.

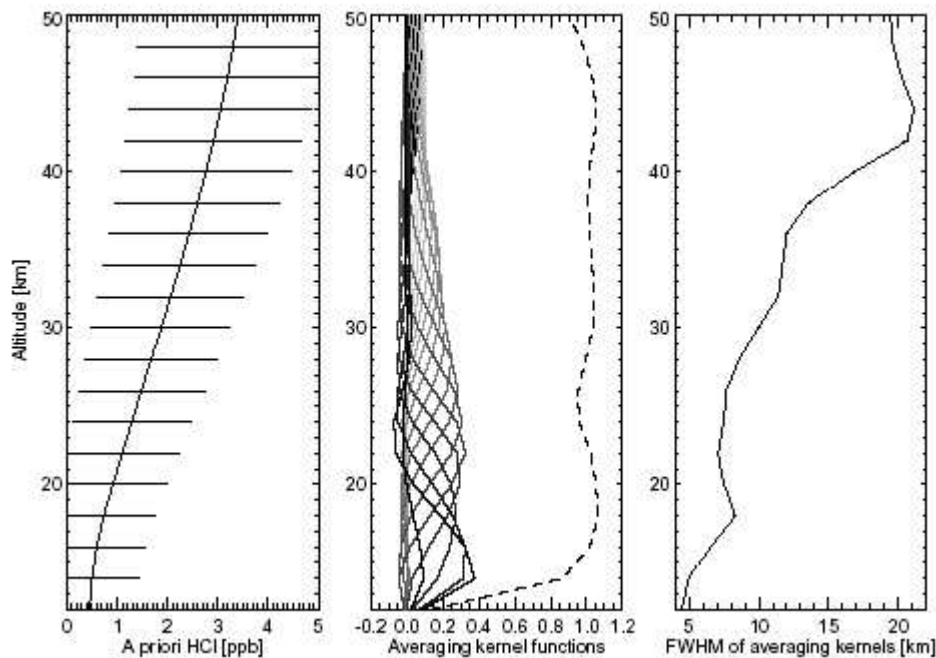


Figure 3.4: Apriori and square root of apriori covariances (left), Averaging kernels and sum of averaging kernels (middle), and altitude resolution of a typical HCl measurement. For a detailed description of the individual plots the reader is referred to figure 3.3. (courtesy Kleinböhl, 2003)

Similarly, as observed in equation 3.16, the altitude range in which sufficient information is contained in ASUR measurements is given by the sum of the averaging kernels for each altitude level. This is equally indicated in figures 3.3-3.5 for ClO, HCl and ozone respectively, and summarized in table 3.2. Since this work used data from the acousto-optical spectrometer (AOS) with a spectral bandwidth of 1.5 GHz and a spectral resolution of 1.5 MHz, profile information is obtained in an altitude range between 15 and 50 km. Where available, the CTS data is avoided since this work is focusing on the lower stratosphere.

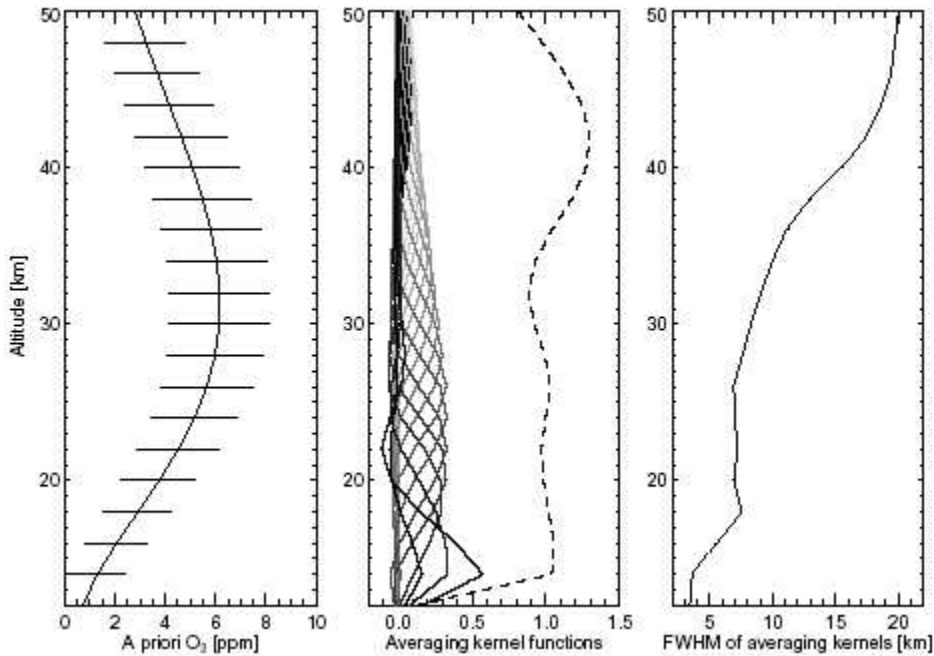


Figure 3.5: A priori and square root of a priori covariances (left), Averaging kernels and sum of averaging kernels (middle), and altitude resolution of a typical ozone measurement by ASUR. For a detailed description of the individual plots the reader is referred to figure 3.3.

Also, an altitude resolution of 5 – 10 km is considered in the lower stratosphere for these retrievals. This is evident from the Full Width Half Maximum (FWHM) of the averaging kernels as shown in figures 3.3-3.5. The FWHM is around 5 – 8 km at the lower end of the retrieved altitude range and it remains around 10 km in an altitude range between 20 and 30 km. This increases further until it reaches values between 15 and 20 km at altitudes between 30 and 40 km.

In these retrievals, the errors emanating from the pressure broadening coefficient and the accuracy of the temperature and pressure data are the main model parameter errors (König, 2001). The latter is particularly evident since the data for altitude-pressure-temperature relation were obtained from different sources for the various campaigns; European Center for Medium range Weather Forecast (ECMWF) and Data Assimilation Office (DAO). These model parameter errors are in addition to the retrieval noise errors resulting from the signal-to-noise ratio. The values are shown in table 3.2.

ASUR measurements have been compared with other instruments in recent years. The major problem is in ASUR CIO measurements, as few instruments measure CIO due to its weak signal. Moreover, in-situ instruments are usually deployed on high-altitude aircraft that cannot fly high enough for a realistic intercomparison with ASUR. However, measurements from a ground-based microwave instrument, Radiometer for Atmospheric Measurements (RAM), have been compared with ASUR CIO (Wohlmann, 2002).

Furthermore, it has been reported that ASUR HCl measurements give results that are approximately 20% higher than the values obtained from other methods (König, 2001). This implies that there are systematic error sources in the ASUR HCl measurement that are not quantified. The observation is accommodated in this study by using a total error of 20% instead of 10% that is actually estimated from the retrieval noise and model parameter errors for ASUR HCl measurements.

Lastly, ASUR error estimates for ozone are found to be reasonable though the measurements are likely higher than most of the other instruments (Bremer, 2002).

4. RESULTS

In this section, the results obtained from this research work shall be presented after summarizing the meteorological conditions that existed during the period when the considered ASUR's measurements were carried out.

4.1 METEOROLOGICAL CONDITIONS

Most of the meteorological conditions presented here are based on winter reports provided by the European Ozone Research Coordinating Unit (EORCU).

The 1994/1995, 1995/1996 and 1996/1997 winters are reported to be very cold with stable vortex and extensive PSCs particularly in 1995/1996 winter. The winter of 1998/99 was the warmest in the 1990s and the area of possible PSCs was the smallest since 1984/85. It was characterized by a major mid-winter warming and the vortex was disturbed for several weeks from around the middle of December. A second major warming started in the upper stratosphere in the second half of February and decreased slowly throughout March. The 1999/2000 winter was one of the coldest since records began in 1964/65. By mid-November the vortex was well established, and the core remained very cold until March. A strong warming in the upper stratosphere in March had little effect at lower levels, where the vortex dominated the polar region until the end of the month. PSCs were detected from mid-November until the first week

of February at 30 hPa, and from the beginning of December until mid-March at 50 hPa, without interruption. In 2002/03 winter, stratospheric temperatures were extremely low in November and December. There was a strong minor warming at the end of December, a major warming in January, and two further minor warmings in February and in March. A late final warming started at the end of March and was complete by late April.

4.2 General Overview of ASUR ClO and HCl Measurements between 1995 and 2003

For a realistic investigation of chlorine activation in the lower stratosphere, it is important to know the altitude where the largest ClO values are found. Shown in figure 4.1 is a contour plot of ASUR's ClO data, produced for all the considered campaigns. This is not a time series but an attempt to illustrate the altitude where the activation is prevalent.

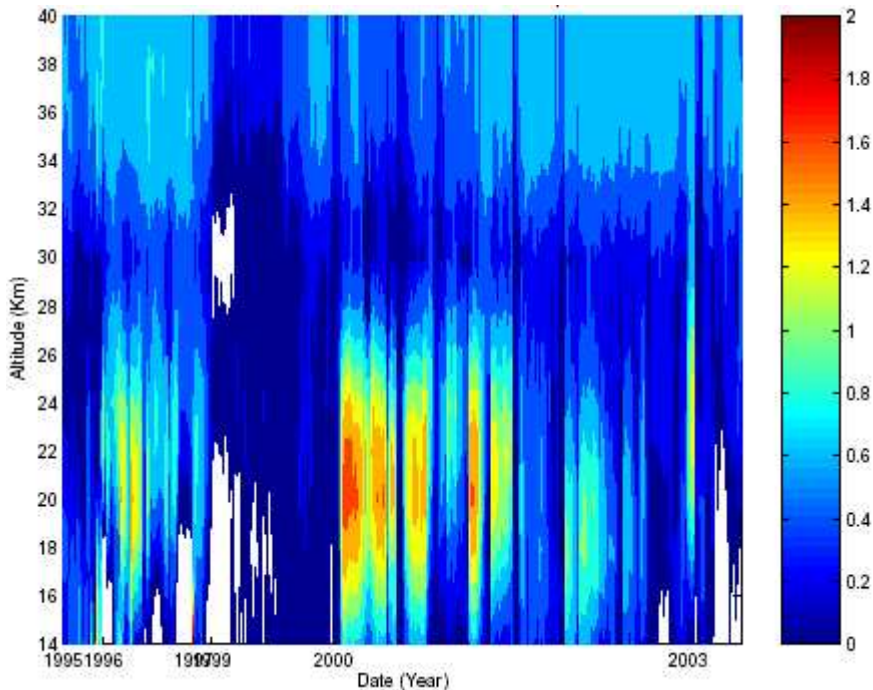


Figure 4.1: ASUR's ClO measurements between 1995 and 2003 polar winters

From figure 4.1, the highest peak for ClO is found around 20 km altitude. It should be noted that this peak might be a result of chemical or dynamical process or both. The white color in figure 4.1 indicates points where there are ‘negative VMR’ due to the retrieval method of ASUR. Since the method minimizes difference between the *a priori* and ASUR measurements, any point with no measurement or below ASUR measurement limit of 0.2 ppb for ClO, may be assigned a negative value by the retrieval method. Also in figure 4.1, a diabatic descent of around 3 km is seen in the winter of 2000. This corroborates earlier studies on vortex descent during the winter of 1999/2000 (Greenblatt et al., 2002; Bremer et al., 2002). The high value in 2003 can be a result of increased cold temperature in January 2003. This is in good agreement with a recently updated SLIMCAT 3-D off-line CTM which confirms that early chemical ozone loss occurred in December 2002 due to extremely low temperatures and early chlorine activation in the lower stratosphere (Feng et al., 2004).

Having established that the highest peak of ASUR ClO measurements is at 20 km (figure 4.1), the volume mixing ratios of ASUR’s ClO and HCl are plotted as functions of temperatures in order to determine the consistency of the data sets with known chemistry in the polar stratosphere. These are shown in figures 4.2 and 4.3 for ClO and HCl respectively.

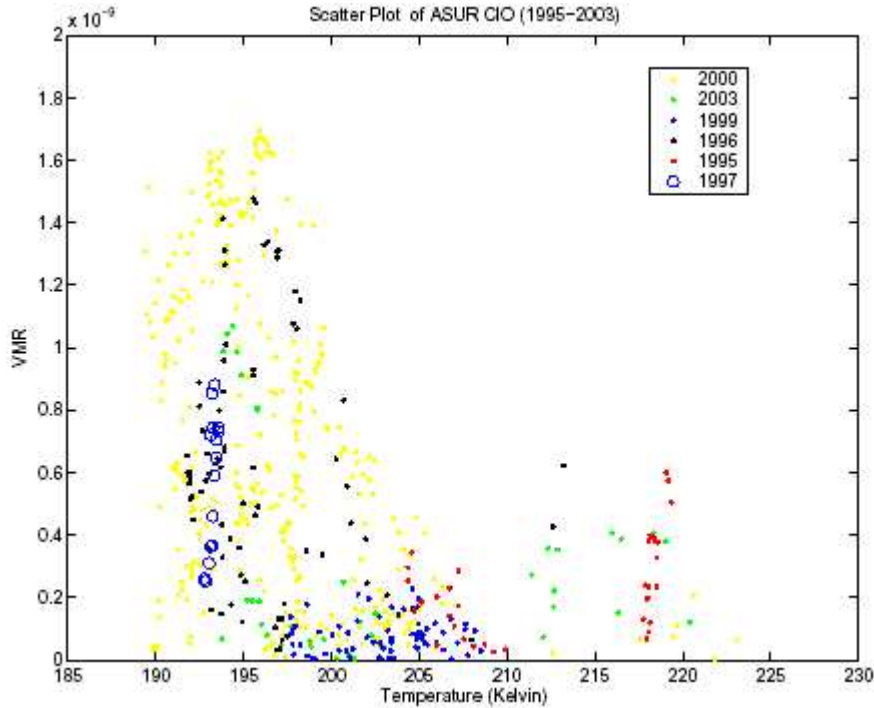


Figure 4.2: ASUR’s ClO measurements as a function of temperature, plotted at 20 km altitude

Although, all the campaigns were carried out in cold seasons, it is not a coincidence in figure 4.2 that the highest values for ClO in all the considered ASUR campaigns (except 1994/1995 and 1998/1999 winters) are found in the region of low temperatures (< 195 K), cold enough for PSCs formation. During 1994/1995 winter, ASUR measurements started in March 1995, and recorded a low chlorine activation that peaks at a period of relatively high temperature. Similarly, since 1998/1999 has been termed a warm winter (WMO, 2000), the highest value was also at higher temperature compared to other cold

winters. The measurements of both winters also (1994/1995 and 1998/1999) show the lowest ClO mixing ratios compared to other winters.

Figure 4.3 gives the corresponding values of HCl for all the campaigns. Also included in figure 4.3 are ASUR measurements in September 2002 (SCIA VALUE, Phase I). This campaign was carried out in the tropics. It is observed that a vmr of 2.7 ppb for HCl in the tropical region at temperature of 220K is reproduced for 1998/1999 winter at a temperature of 199K which is high enough to prevent PSCs formation. This underscores the ‘warmness’ of 1998/1999 winter.

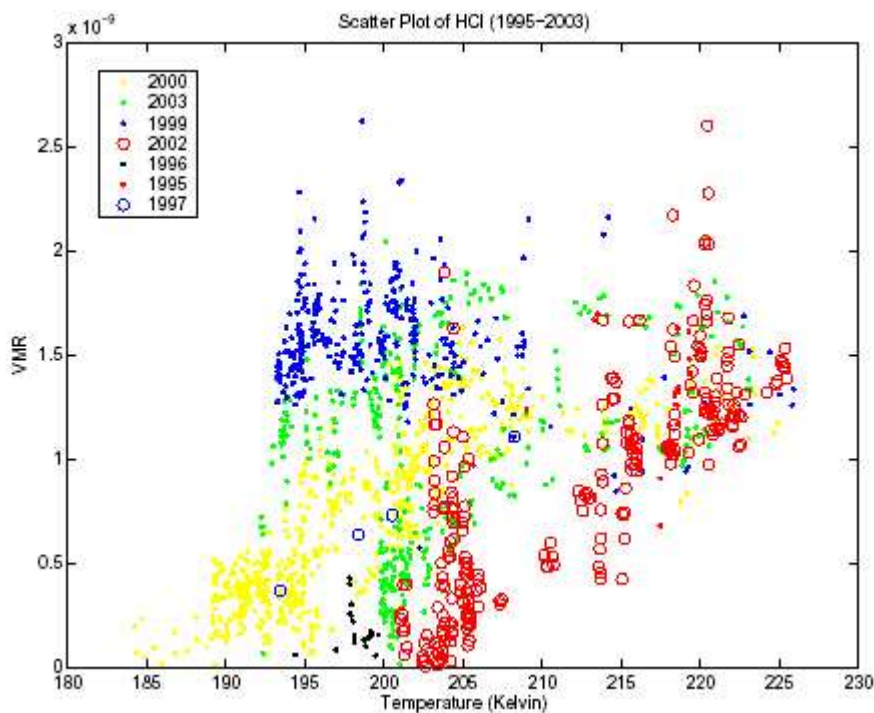


Figure 4.3: ASUR’s HCl measurements as a function of temperature, plotted at 20 km altitude

Figure 4.4 gives the sum of ClO and HCl. The data is binned at 5° equivalent latitude (eql). The maximum sum of ClO and HCl (green) on this plot is 2.7 ppb. This is a reasonable value compared to model result of 2.4 ppb for ClO_y for this altitude region (from personal discussion between Bremer, H and Sinnhuber, B-M). The blue and red lines give the error bars (1σ) for HCl and ClO respectively. As it shall be seen in subsequent results, the use of equivalent latitude (eql) instead of normal latitude becomes

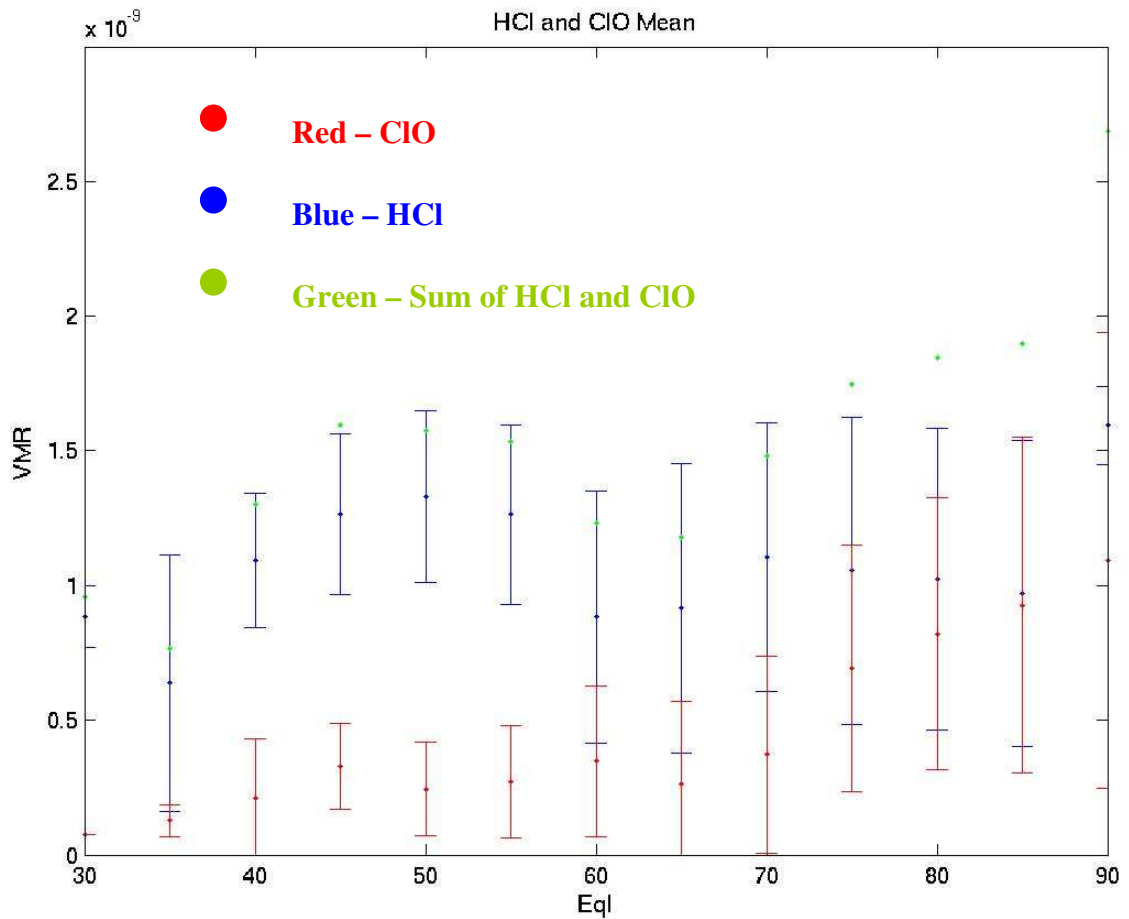


Figure 4.4: Sum of ClO and HCl with their individual mixing ratios at 20 km altitude

necessary since the northern pole and the arctic vortex are not aligned. The vortex often tilts to the east of the northern pole, thereby giving rise to inadequacy of normal latitude for a reasonable intercomparison between different measurements.

4.3 Seasonal Variation Of ASUR's ClO and HCl Measurements

Figures 4.5 and 4.6 show ASUR's ClO and HCl respectively as functions of day of the year during the period normally expected to witness activation and deactivation of chlorine during winter in the polar stratosphere. The general impression of these two figures correlate with figure 1.4 which illustrates how ClO increases as HCl decreases by reacting with ClONO₂.

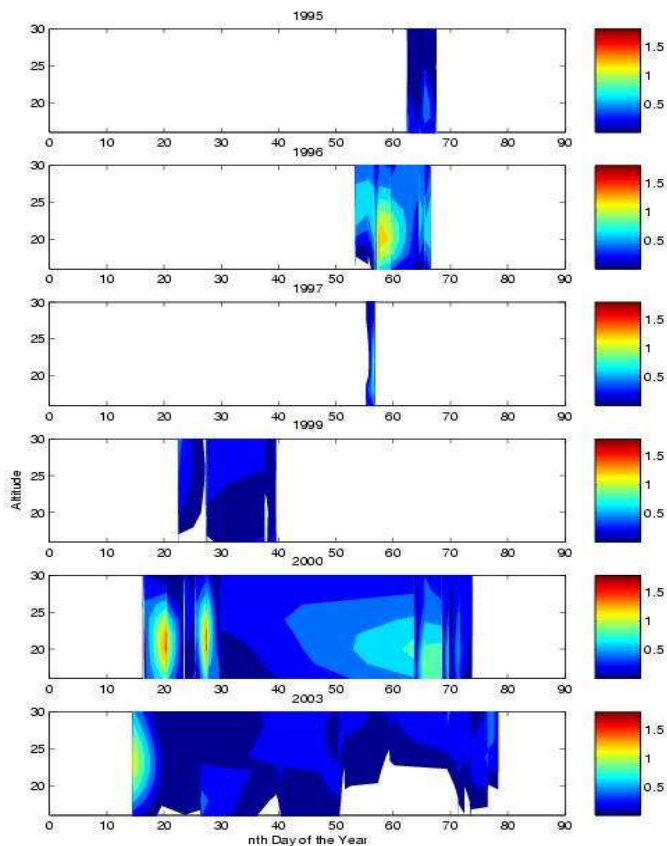


Figure 4.5: Variation of ASUR's ClO with day of the year

Except for 1999, all measurements carried out by ASUR in January show extensive chlorine activation. This is evident in 2000 and 2003 winters. This activation is equally recorded for measurements in March as shown in 1996 and 2000 winters, while the break up of the vortex in February 2003 may account for the low ClO mixing ratio in March 2003.

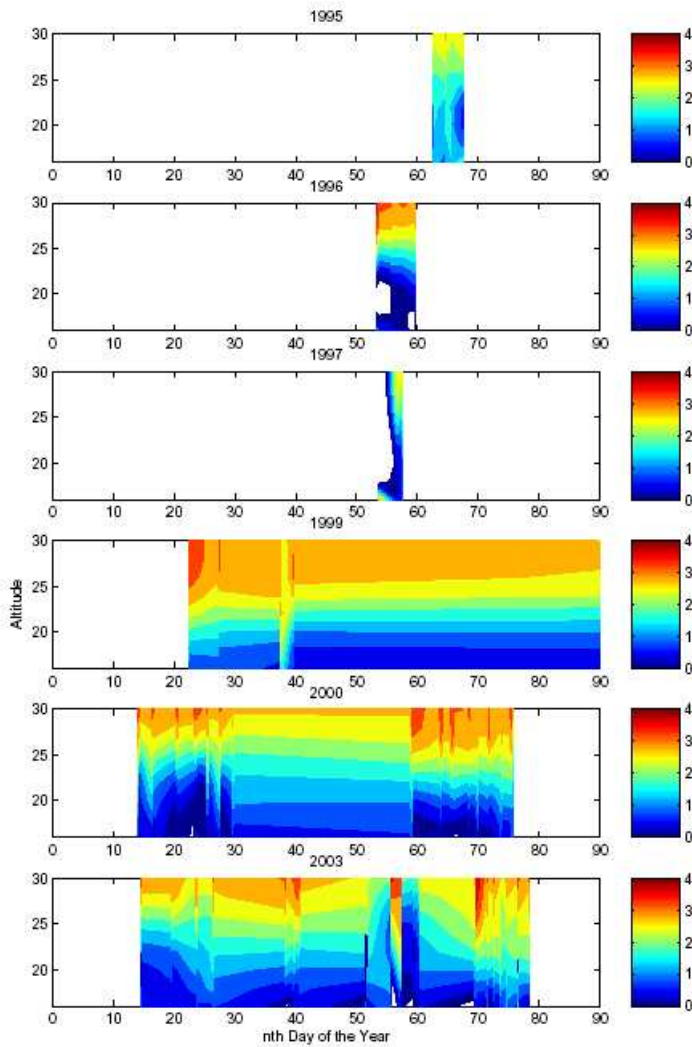


Figure 4.6: Variation of ASUR’s HCl with day of the year.

4.4 . Latitudinal Variation of ASUR CIO and HCl Measurements

Figures 4.7 and 4.8 show the variation of ASUR's CIO and HCl with equivalent latitude, respectively. Although the solar zenith angle (SZA) is not necessary for HCl, it is equally used in order to have a comparable idea of how volume mixing ratios change with latitude in the ASUR measurements for the considered winters.

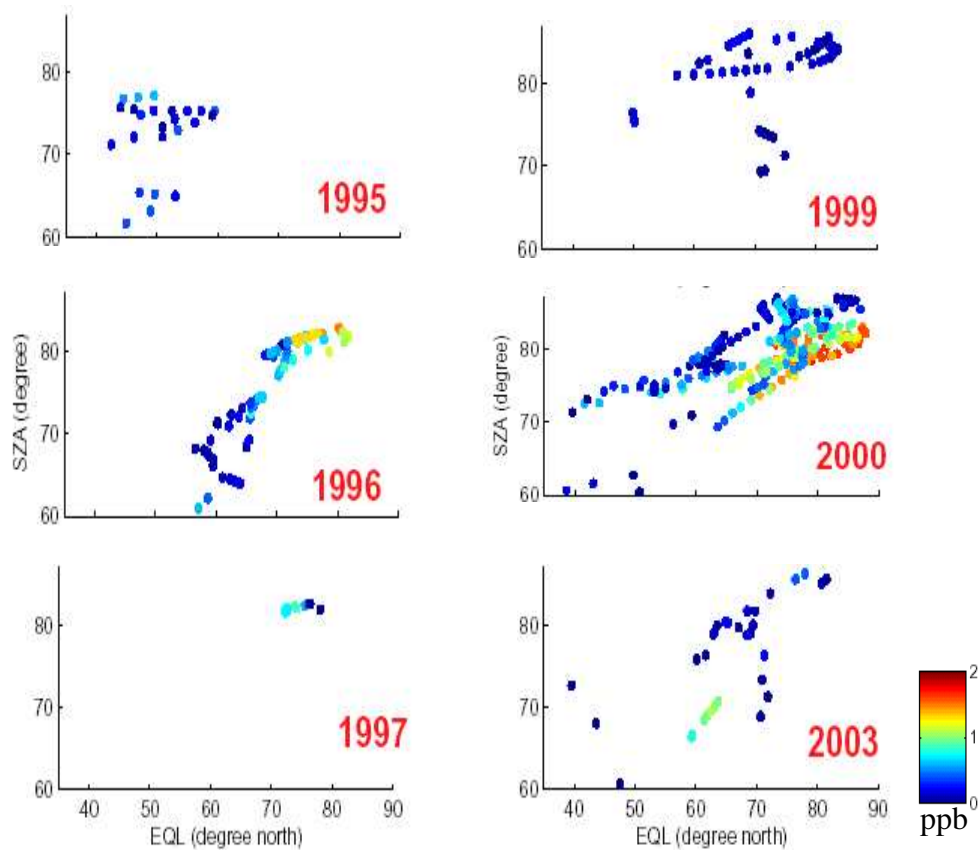


Figure 4.7: Variation of ASUR's CIO with equivalent latitude

In figure 4.7, the lower latitudes record low mixing ratios for ClO and this gradually increases towards the mid latitude and peaks at the polar region. Exceptions are found in 1997 and 1999. The low values at high latitudes observed in 1997 for ClO may be due to ASUR's few measurements at that time, capturing only low activation of chlorine. Also, as it has been indicated that 1999 was an unusual winter, this reflected in the low values obtained by ASUR at high latitudes in 1999. Moreover in 2003, a high volume mixing

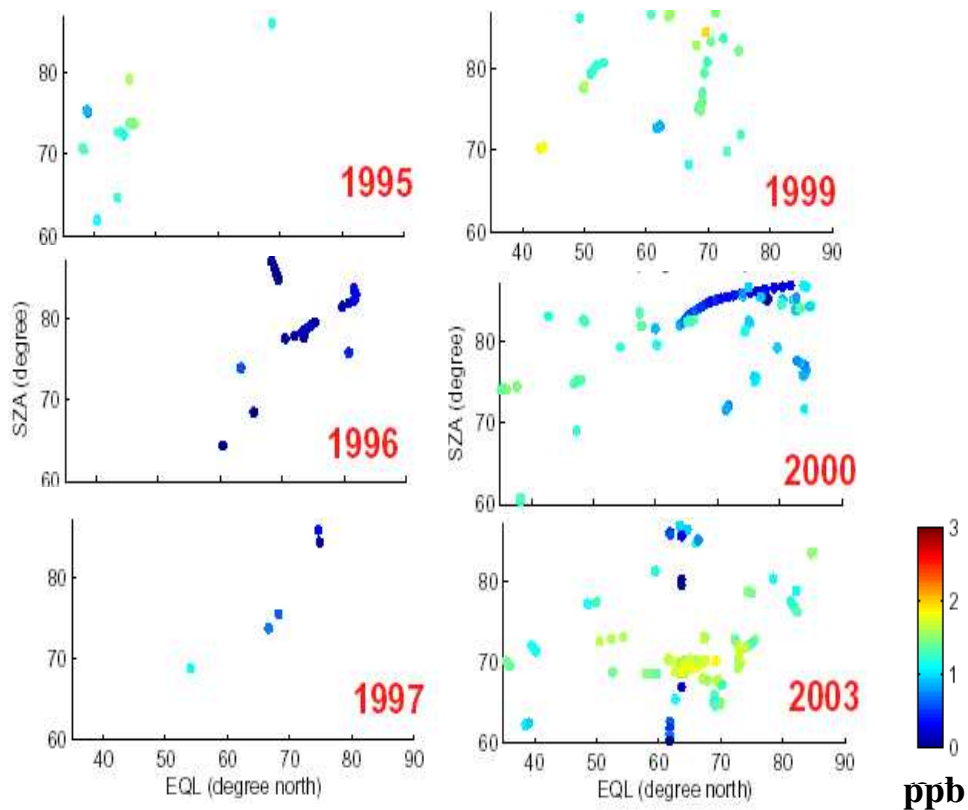


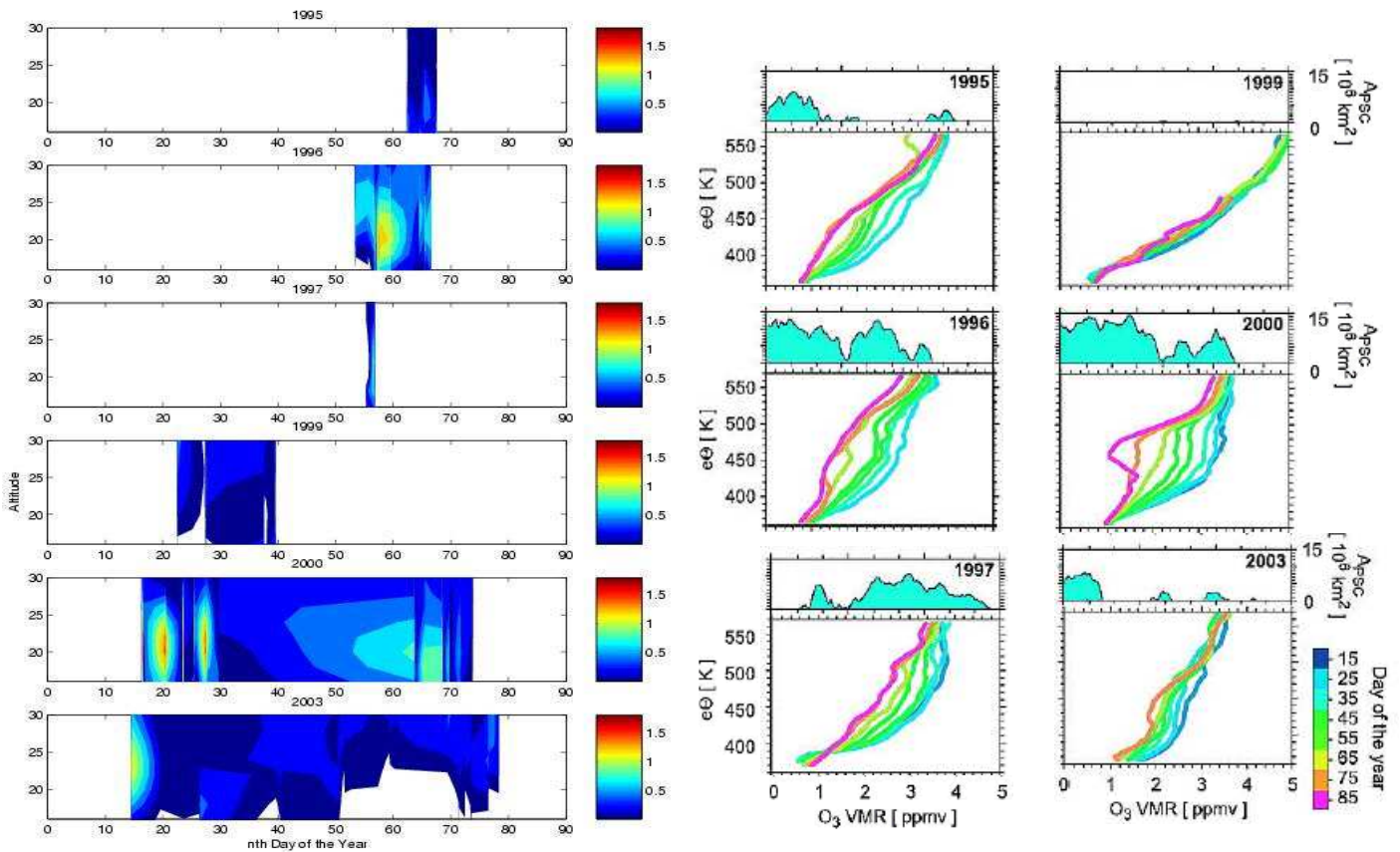
Figure 4.8: Variation of ASUR's HCl with equivalent latitude

ratio of ClO of around 1.2 ppb was found between 61° and 64° latitude. This corresponds to the vortex edge and raises question if there is activation in that region. However, it is not chlorine activation but a result of the dynamical processes due to the stratospheric major sudden warming observed in February 2003.

In figure 4.8, nearly a sharp contrast to figure 4.7 is found; the lower latitudes record high mixing ratios for HCl and it gradually decreases towards the mid latitude and reaches lowest values at the polar region. A major exemption is the 2003 winter. The reason for high HCl values at high latitudes in 2003 can be attributed to the meteorological situation as stated for ClO.

4.5 Comparison of ASUR CIO with other instruments and model results

Results from ASUR CIO are compared with the arctic ozone loss (Rex et al., 2004). This is the result of analyses comprising about 2000 ozone soundings within the arctic polar



(a)

(b)

Figure 4.9: (a) same as figure 4.5. (b) Top panel shaded light green: Geographical area covered by temperatures below T_{NAT} (A_{PSC}) for 6 winters. Colored curves: Evolution of the vortex averaged ozone mixing ratio through the same winters (Rex et al., 2004).

vortex to quantify chemical loss of ozone in the last winters. ASUR's ClO is also compared with total ozone reduction in the vortex derived from ground based measurements and simulations by the REPROBUS and SLIMCAT models (Goutail et al.,

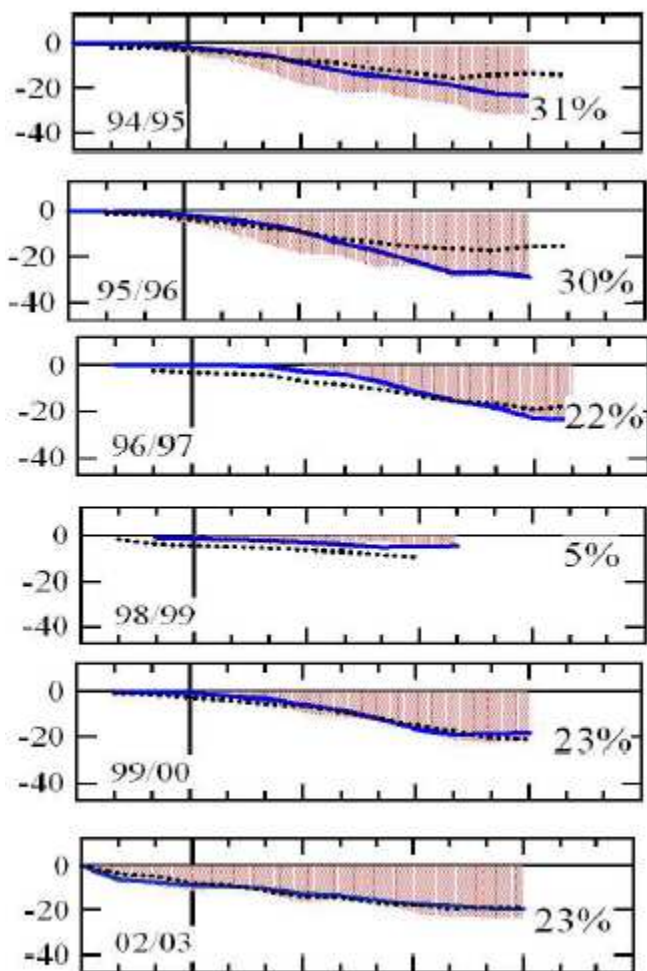


Figure 4.10: Total ozone reduction in the vortex obtained from the measurements of the SAOZ stations (shaded pink) and simulated by REPROBUS (blue solid line) and SLIMCAT (black dotted line) for 1994/1995, 1995/1996, 1996/1997, 1998/1999, 1999/2000 and 2002/2003 winters. (Goutail et al., 2004).

2004). The ground based data are total ozone columns measured at seven Arctic stations equipped with SAOZ UV-visible spectrometers, part of the Network for the Detection of Stratospheric Changes (NDSC).

The low value of ASUR ClO mixing ratio during winter 1995 can be a result of low chlorine activation at the time of ASUR measurement. Although all other instruments and models record high chemical ozone loss, ASUR measurements started when the PSCs have nearly disappeared, as indicated in figure 4.9 (b). The 1996 ClO vmr of around 1.4 ppb obtained from ASUR is in good agreement with large PSC formation and high ozone destruction from the sonde results. It is also consistent with the 30% ozone reduction from the SAOZ instruments and the model results, despite the discrepancy between the two models. However, as a result of few measurements in late February of 1997, ASUR ClO result is not comparable with any of the instruments or model calculations results for ozone. As noted earlier, the meteorological situation of 1999 winter did not permit formation of PSCs. This resulted in nearly no ozone loss in the sonde results, and low values of ASUR ClO. It is equally captured by the models and SAOZ instruments with maximum loss of 5%. This is relatively very low. The winter of 2000 was one of the coldest in recent years. This situation was represented by the large ozone destruction observed from the compared instruments and models, and the high ClO mixing ratio in ASUR results. Lastly in 2003, the situation is reported to be similar to 2000 winter by the SAOZ instruments and model results. However, ASUR recorded another high value for

CIO (although lower than winter of 2000) and this conforms with the ozone loss values obtained from the sonde results.

4.6 DISCUSSION AND CONCLUSIONS

From the ASUR data analyzed in this project, there is a strong evidence of considerable interannual variability in the timing and magnitude of chlorine activation in the lower stratosphere during winter. Also there is a tremendous anti-correlation between ASUR CIO results and ozone results from other instruments and models. Seasonal and latitudinal variation of CIO and HCl are also observed by ASUR.

The discrepancy between ASUR's observation (2.7 ppb) in figure 4.4 and the expected maximum sum of HCl and CIO (< 2.4 ppb) may be due to two reasons. The lower value of 2.4 ppb may mean that part of the reactive chlorine has been converted to ClONO₂ by reaction of CIO and NO₂. Also, it could be due to higher tropopause, for example closer to mid and tropical latitudes. This will naturally result in a slight upward movement of the stratospheric airmass compared to polar regions, thereby giving rise to lower CIO_y. However, the high value obtained from ASUR's result could be due to the time of measurements. Perhaps, ASUR measurements were carried out during the time when the

vortex exists and later in the winter, this implies subsidence of air mass, thereby giving rise to high ClO_y value.

In figure 4.7 and 4.8, the high HCl value at high latitudes and 'virtual' chlorine activation at the vortex edge in 2003 winter has been linked to the dynamical processes. Perhaps the vortex edge became weak due to the sudden warming which could have resulted in exchange of high and mid-latitude air. This could transport HCl-rich air into high latitudinal region and ClO -rich air around the vortex edge.

SUMMARY

Emissions of chlorine compounds into the atmosphere by anthropogenic activities destroy the stratospheric ozone layer; thereby monitoring the concentration of these compounds becomes necessary in order to investigate any observed evolution, and to verify compliance with different international protocols banning their production by human processes. Many of these chlorine species show strong spectral features at submillimeter wavelengths and can therefore be measured using microwave remote sensing techniques. The instrument used for this study is the Airborne Submillimeter Radiometer ASUR. It measures thermal emission lines of a variety of atmospheric trace gases related to chlorine chemistry in the stratosphere e.g HCl- the chlorine reservoir gas, ClO- which is very efficient for catalytic ozone destruction in the lower stratosphere during winter, N₂O - the chemically inert trace gas suitable to differentiate between chemical and dynamical processes, and ozone among others. The spectral range of ASUR is between 604.3 and 662.3 GHz. By using a non-linear least squares inversion technique, volume mixing ratio profiles were retrieved from the spectrally resolved pressure broadened lines. This research work focused on chlorine activation in the arctic winters over the past years by evaluating the time series from 1995 to 2003. Evidence of a large chemical ozone losses and a strong, spatially variable chlorine activation with high ClO and low HCl mixing ratios were observed.

ACKNOWLEDGEMENT

My sincere gratitude goes to my supervisor, Prof. Justus Notholt, whose magical touch and professional contributions served as sources of inspiration for me throughout this MSc thesis. I would like to thank Dr. Harry Küllmann for his support and beautiful discussions, also Dr. Armin Kleiböhl and Jayanarayanan Kuttippurath for their advice and fantastic working relationship. Then to Dr. Holger Bremer, who amazed me throughout my MSc thesis with his priceless magnanimity which is difficult to describe, I appreciate everything.

I am thankful to Dr. Miriam Sinnhuber whose former work in ASUR group laid a good foundation for my MSc thesis, and also for her informal direct and indirect contributions.

I am thankful to Dr. Björn-Martin Sinnhuber for his many unsolicited scientific advice, and for providing the routine which I used in calculating the solar zenith angle for my thesis. Furthermore, I would like to thank my wife and daughter for their numerous sacrifices and utmost perseverance throughout the duration of this programme. I will always love both of you. I thank my friends and everybody who supported me in one way or the other during my MSc programme.

Finally, I thank the organizers of the Postgraduate Programme in Environmental Physics for my admission to the MSc Environmental Physics programme, particularly Prof. Jörn Bleck-Neuhaus, Messrs Stefanie Bühler and Barbara Kozak, for their unrelenting efforts

which made it possible for me to attend the course. The swift response of Ms. Christine Schiwiek to all administrative matters cannot go unappreciated. I thank all of you.

REFERENCES

Andrews, D.G., Holton, J.R. and Leovy, C.B., 1987: Middle Atmosphere Dynamics. New York: Academic Press.

Brasseur, G. P., Orlando, J. J. and Tyndall, G. S., 1999: Atmospheric chemistry and global change. Oxford University Press.

Brasseur, G. P. and Solomon, S., 1986: Aeronomy of the middle atmosphere. Dordrecht: D. Reidel Publishing Company.

Bremer, H., von König, M., Kleinböhl, A., Küllmann, H., Künzi, K., Bramstedt, K.,

Burrows, J.P., Eichmann, K.-U., Weber, M. and Goede, A. P.H., 2001: Ozone depletion observed by ASUR during the Arctic Winter 1999/2000.

Bremer, H., 2002: Messungen von dynamischen Tracern und Ozon in der arktischen Stratosph: Analyse und Interpretation flugzeuggetragener Submillimeterwellenmessungen, PhD thesis University of Bremen.

Bühler, S., 1999: Microwave Limb Sounding of the Stratosphere and Upper Troposphere. Phd thesis, University of Bremen.

Bühler, S., von Engel, A., Urban, J., Wohlgemuth, J. Küünzi, K.F., 1999: The impact of cirrus clouds, ESTEC. Contract No 12053.

Chapman, S., 1930: On ozone and atomic oxygen in the upper atmosphere. (Phylos. Mag.), 369.

Chipperfield, M. and Pyle, J., 1998: Model sensitivity studies of Arctic ozone depletion. J. Geophys. Res., **103**, 28389-28403.

EORCU, 1999: *The northern hemisphere stratosphere in the winter and spring of 1998/1999*. European Ozone Research Coordination Unit. Available on <http://www.ozone-sec.ch.cam.ac.uk/>.

EORCU, 2000: *The northern hemisphere stratosphere in the winter and spring of 1999/2000*. European Ozone Research Coordination Unit. Available on <http://www.ozone-sec.ch.cam.ac.uk/>.

EORCU, 2003: *The northern hemisphere stratosphere in the 2002/03 winter*. European Ozone Research Coordination Unit. Available on <http://www.ozone-ec.ch.cam.ac.uk/>.

Feng, W., Chipperfield, P., Davies, S., Sen, B., Toon, G., Blavier, J.F., Webster, C.R., Volk, C.M., Ulanovsky, A., Ravagnani, F., von der Gathen, P., Jost, H., Richard, E.C and Claude, H., 2004: Three-dimensional model study of the arctic ozone loss in 2002/2003 and comparison with 1999/2000 and 2003/2004, Atmos. Chem. Phys.

Discuss, **4**, 5045–5074.

Fahey, D.W., Gao, R.S., Carslaw, K.S., Kettleborough, J., Popp, P.J., Northway, M.J., Holecek, J.C., Ciciora, S.C., McLaughlin, R.J., Thompson, T.L., Winkler, R.H., Baumgardner, D.G., Gandrud, B., Wenneberg, P.O., Dhaniyala, S., McKinney, K., Peter, T., Salawitch, R.J., Bui, T.P., Elkins, J.W., Webster, C.R., Atlas, E.L., Jost, H., Wilson, J.C., Herman, R.L., Kleinböhl, A. and von König, M., 2001: The Detection of Large HNO₃-Containing Particles in the Winter Arctic Stratosphere. *Science*, **291**, 1026–1031.

Farman, J.C., Gardiner, B.G. Shanklin, J.D., 1985: Large losses of total ozone in Antarctica reveal seasonal ClO_x/NO_x interaction. *Nature*, **315**, 207–210.

Goutail, F., Pommereau, J.-P., Lefevre, F., Van Roozendaal, M., Andersen, S.B., Kastad Høiskar, B.-A., Dorokhov, V., Kyro, E., Chipperfield, P. and Feng, W., 2004: Early unusual ozone loss during the Arctic winter 2002/2003 compared to other winters, *Atmos. Chem. Phys. Discuss*, **4**, 5019–5044.

Holton, J.R., 1992: *An Introduction to Dynamic Meteorology*. Academic Press.

Holton, J.R., Haynes, P.H., McIntyre, M.E., Douglas, A.R., Rood, R.B. and Pfister, L., 1995: Stratosphere-troposphere exchange. *Rev. Geophys* **33**, 403–439.

von König, M., 2001: Chloraktivierung und PSC-Bildung in der arktischen Stratosphäre: Analyse und Interpretation flugzeuggetragenen Submillimeterwellenmessungen}. Phd thesis, Universität Bremen.

- von König, M., Bremer, H., Eyring, V., Goede, A., Hetzheim, H., Kleipool, Q., Küllmann, H. and Künzi, K., 2000: An Airborne Submm Radiometer for the Observation of Stratospheric Trace Gases. In *Microwave Radiometry and Remote Sensing of the Earth's Surface and Atmosphere*, Pampaloni, P. and Paloscia, S., VSP Utrecht.
- Mees, J., Crewell, S., Nett, H., de Lange, G., van den Stadt, H., Kuipers, J.J. and Panhuyzen, R.A., 1995: ASUR - An Airborne SIS receiver for Atmospheric Measurements of Trace Gases at 625 to 760 GHz. *IEEE Trans. Microwave Theory and Techniques*, **43**.
- Molina, J.M. and Rowland, F.S., 1974: Stratospheric sink for chlorofluoromethans: Chlorine catalyzed destruction of ozone. *Nature*, **249**, 810-812.
- Rex, M., Salawitch, R. J., von der Gathen, P., Harris, N. R. P., Chipperfield, P and Naujokats, B., 2004: Arctic ozone loss and climate change, *Geo. Res. Lett*, **31**, 4116-4119
- Rodgers, C.D., 1976: Retrieval of atmospheric temperature and composition from remote measurements of thermal radiation. *Rev. Geophys. Space Phys.*, **14**, 609-624.
- Rodgers, C.D., 1990: Characterization and error analysis of profile retrieval from remote sounding measurements. *J. Geophys. Res.*, **95**, 5587-5595.
- Rosolen, C., Dierich, P., Michet, D., Lecacheaux, A., Palacin, F., Robiliard, R., Rigeaud, F. and Vola, P., 1994: *Wideband acousto optical spectrometer*. final report on

workpackage 2411, ESA.

- Sinnhuber, B.-M., Chipperfield, M.P., Davies, S., Burrows, J.P., Eichmann, K.-U., Weber, M., von der Gathen, P., Guirlet, M., Cahill, G., Lee, A. and Pyle, J., 2000: Large loss of total ozone during the Arctic winter of 1999/2000. *Geophys. Res. Lett.*, **27**, 3473-3476.
- Urban, J., 1997: Messungen der stratosphärischen Spurengase ClO, O₃, N₂O, H₂O und OH mittels flugzeuggetragener Submillimeterwellen-Radiometrie bei 650 und 2500 GHz. Phd thesis, Universität Bremen.
- Vowinkel, B., 1988: Passive Mikrowellenradiometrie. Braunschweig: Friedr. Vieweg & Sohn Verlagsgesellschaft mbH.
- Wallace, J.M. and Hobbs, P.V., 1977: Atmospheric Science. New York: Academic Press.
- WMO, 1995: Scientific Assessment of Ozone Depletion: 1994. Global Ozone research and Monitoring Project-37, World Meteorological Organization.
- WMO, 2000: Scientific Assessment of Ozone Depletion: 1999. Global ozone research and monitoring project, World Meteorological Organization.

